Here we present full results for C1-C26 in Figures S 1– S 35 in terms of the vorticity contours, lift and drag measurements and, where applicable, Fourier transforms. Results for additional tandem simulations are presented in figures S 36 and S 37 and in Table S 1 at Re = 3900: AS1 and AS2 for $\frac{L}{D} = 1.25$ and for $\frac{L}{D} = 1.025$ respectively.

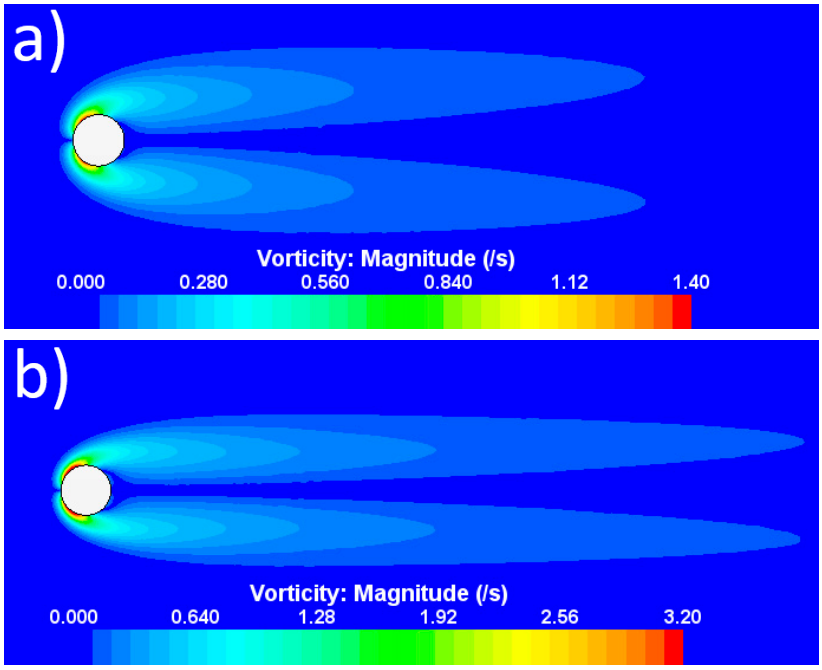

Figure S1. *Vorticity contours of a) C1 at Re = 20; b) C2 at Re = 40.*

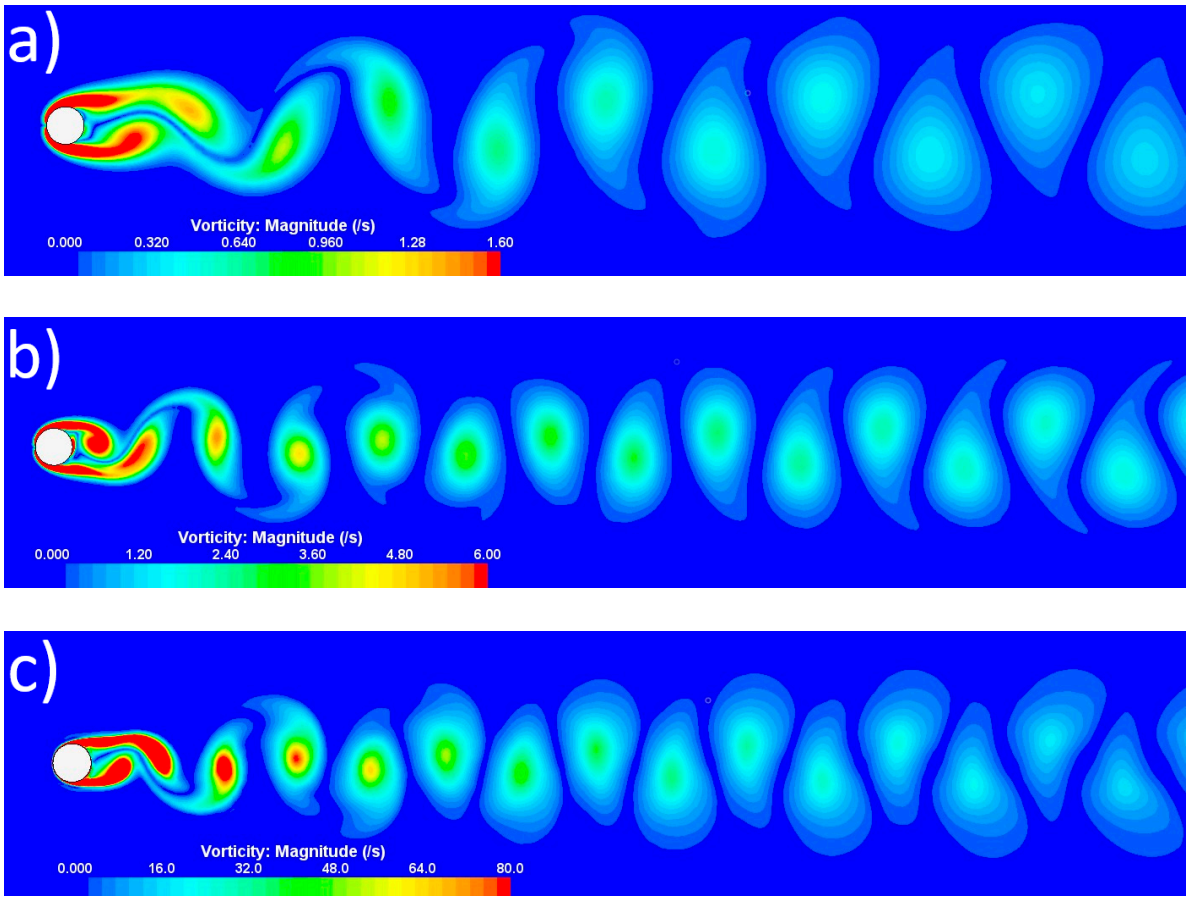

Figure S2. *Vorticity contours of a) C3 at Re = 80; b) C4 at Re = 200; c) C5 at Re = 3900.*

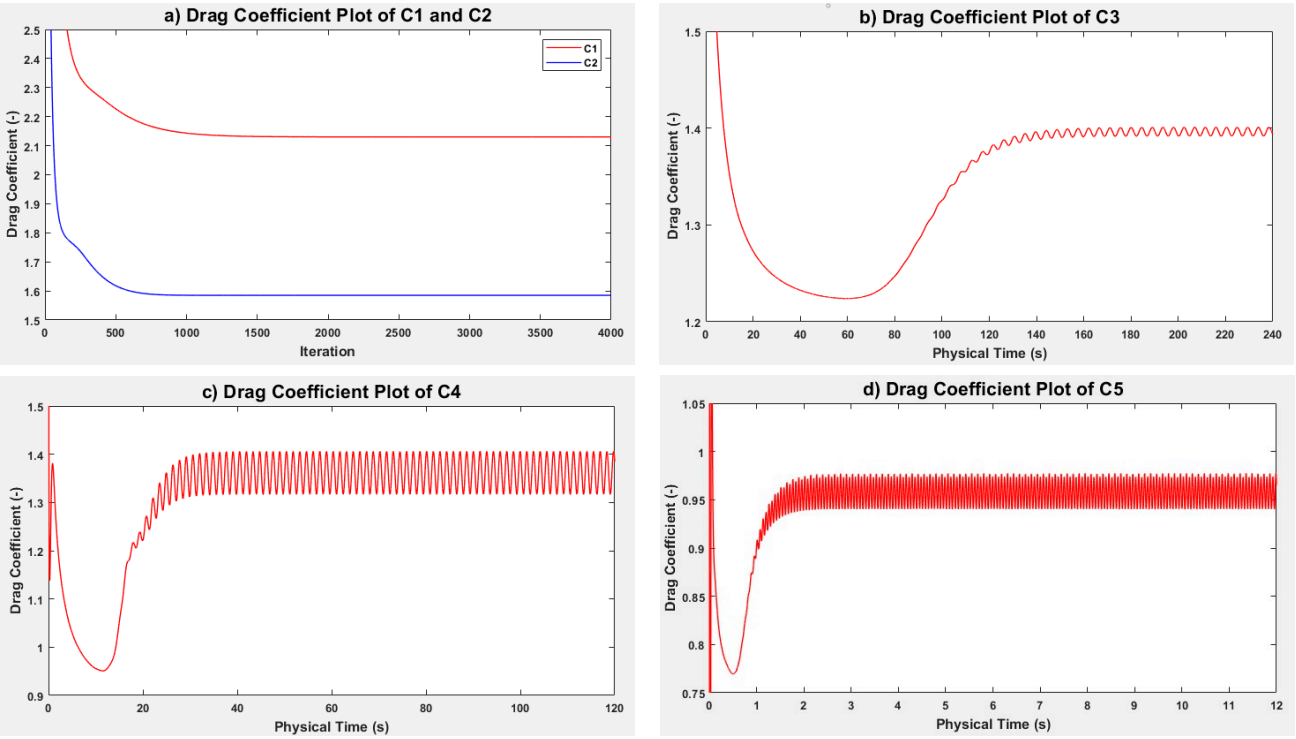

Figure S3. *Drag coefficient plot of a) C1 at Re = 20 and C2 at Re = 40; b) C3 at Re = 80; c) C4 at Re = 200; d) C5 at Re = 3900.*

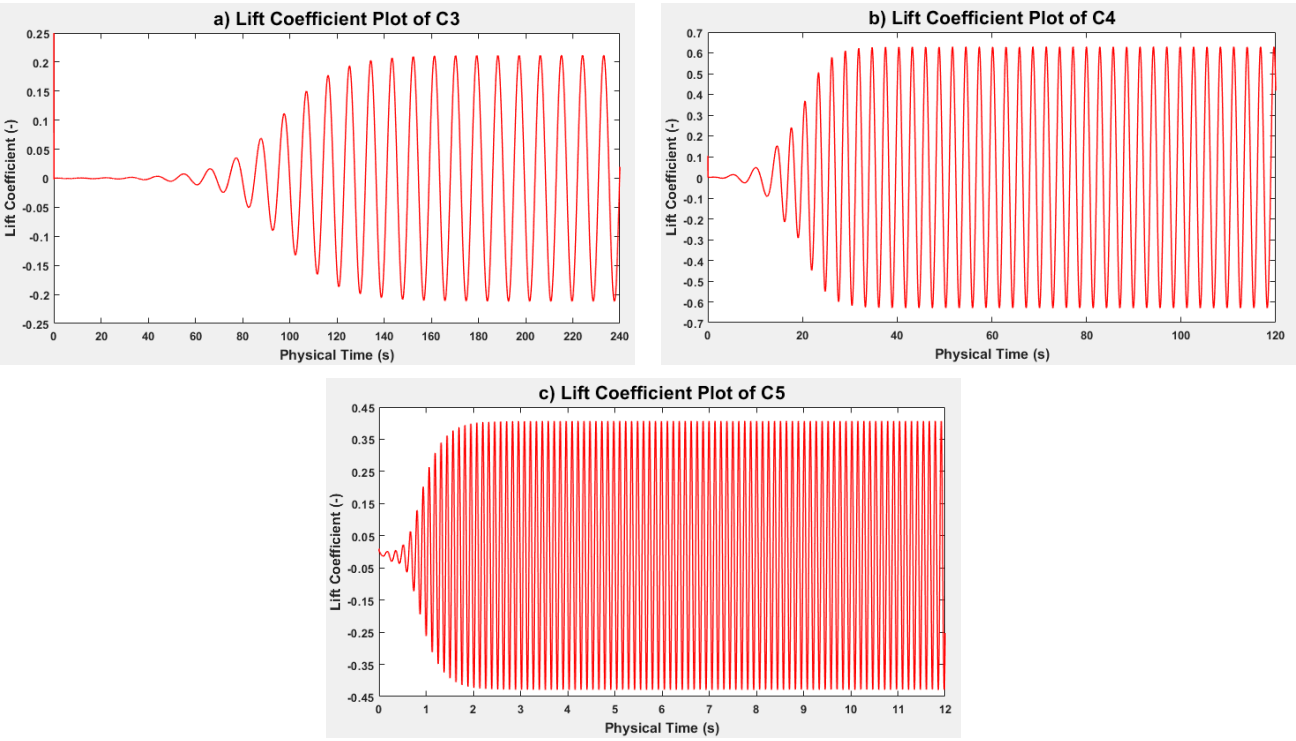

Figure S4. *Lift coefficient plot of a) C3 at Re = 80; b) C4 at Re = 200; c) C5 at Re = 3900.*

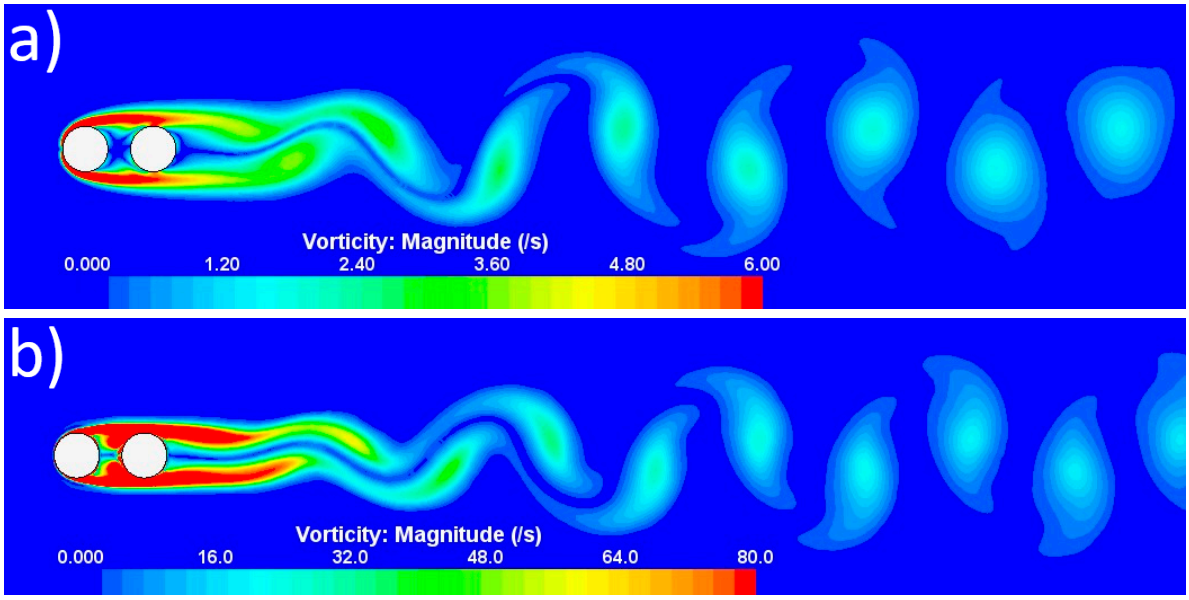

Figure S5. *Vorticity contours of a) C6 at Re = 200; b) C7 at Re = 3900.*

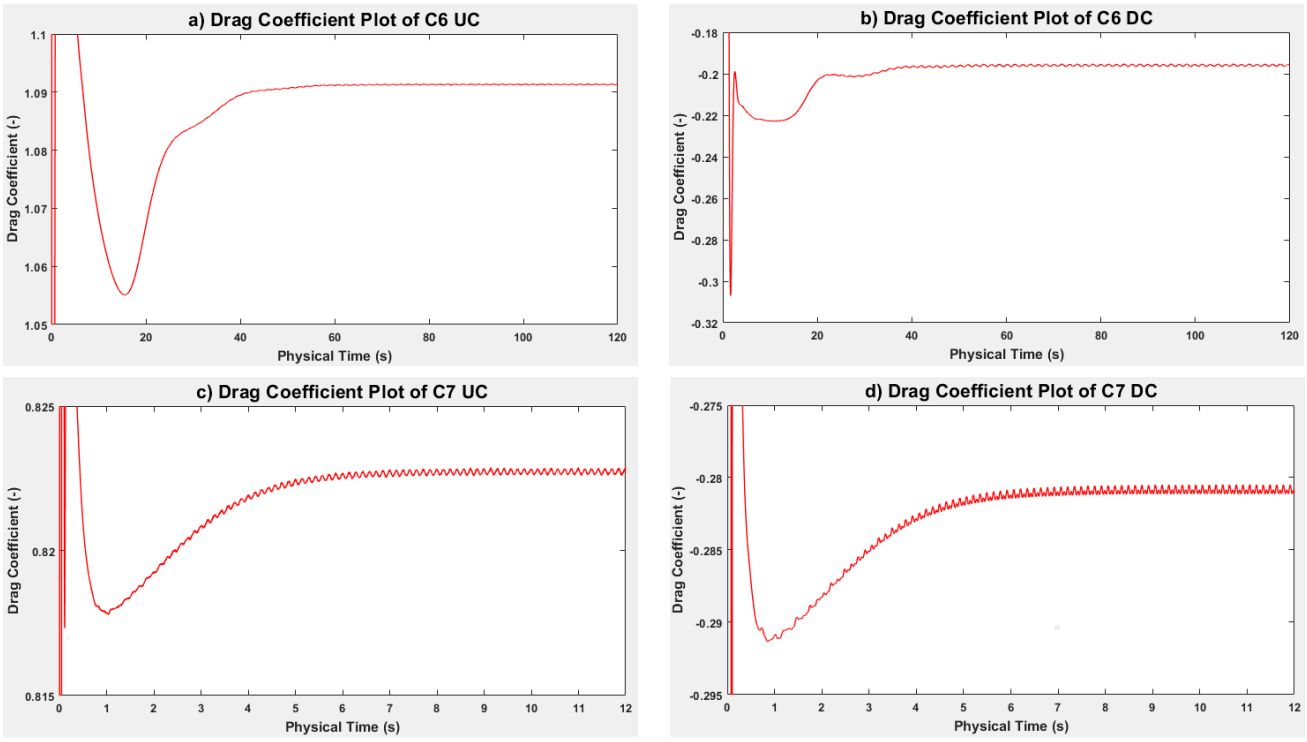

Figure S6. *Drag coefficient plot of a) C6 UC at Re = 200; b) C6 DC at Re = 200; c) C7 UC at Re = 3900; d) C7 DC at Re = 3900.*

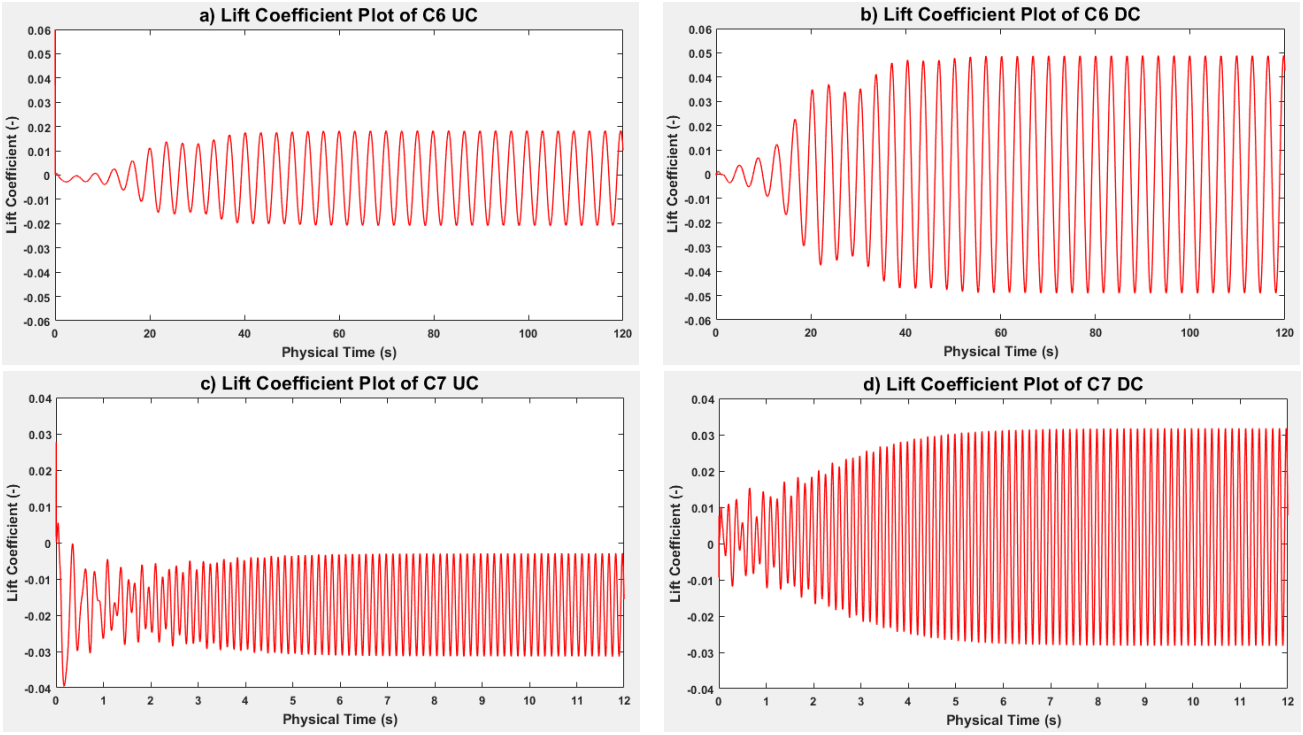

Figure S7. *Lift coefficient plot of a) C6 UC at Re = 200; b) C6 DC at Re = 200; c) C7 UC at Re = 3900; d) C7 DC at Re = 3900.*

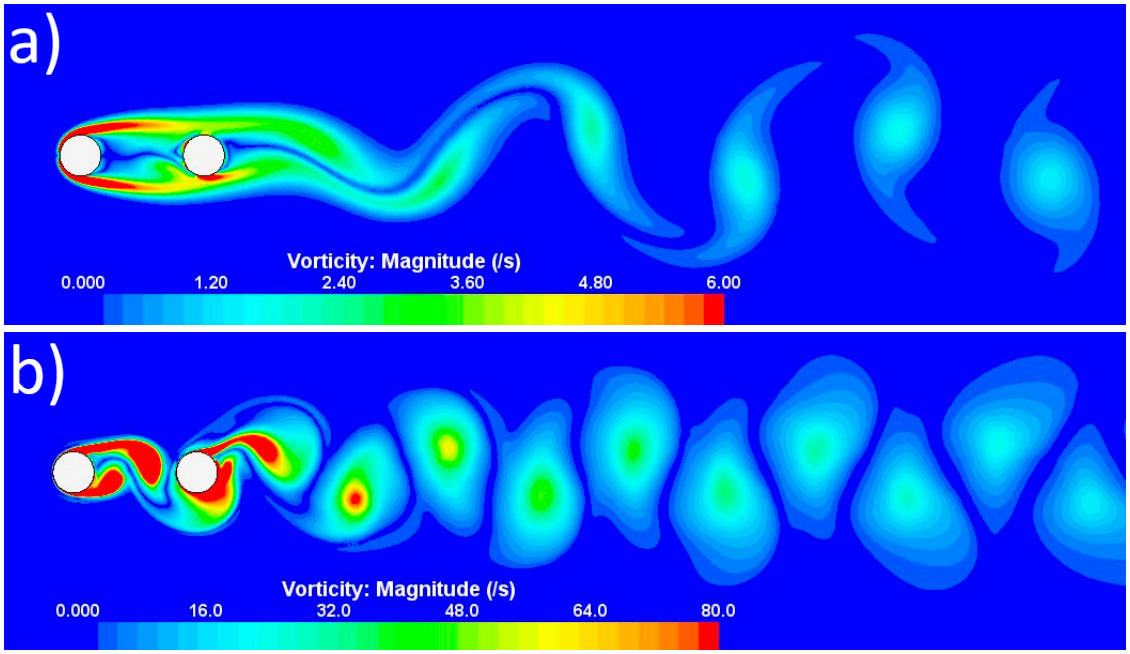

Figure S8. *Vorticity contours of a) C8 at Re = 200; b) C9 at Re = 3900.*

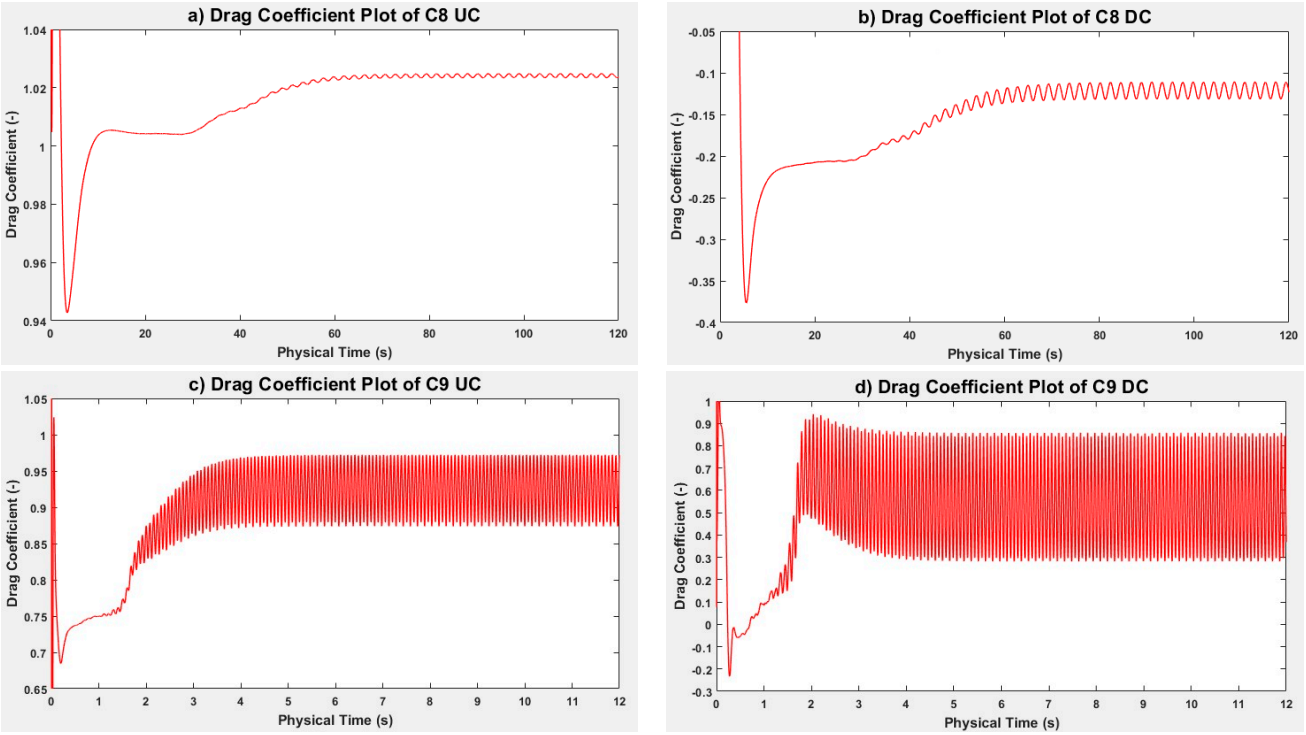

Figure S9. *Drag coefficient plot of a) C8 UC at Re = 200; b) C8 DC at Re = 200; c) C9 UC at Re = 3900; d) C9 DC at Re = 3900.*

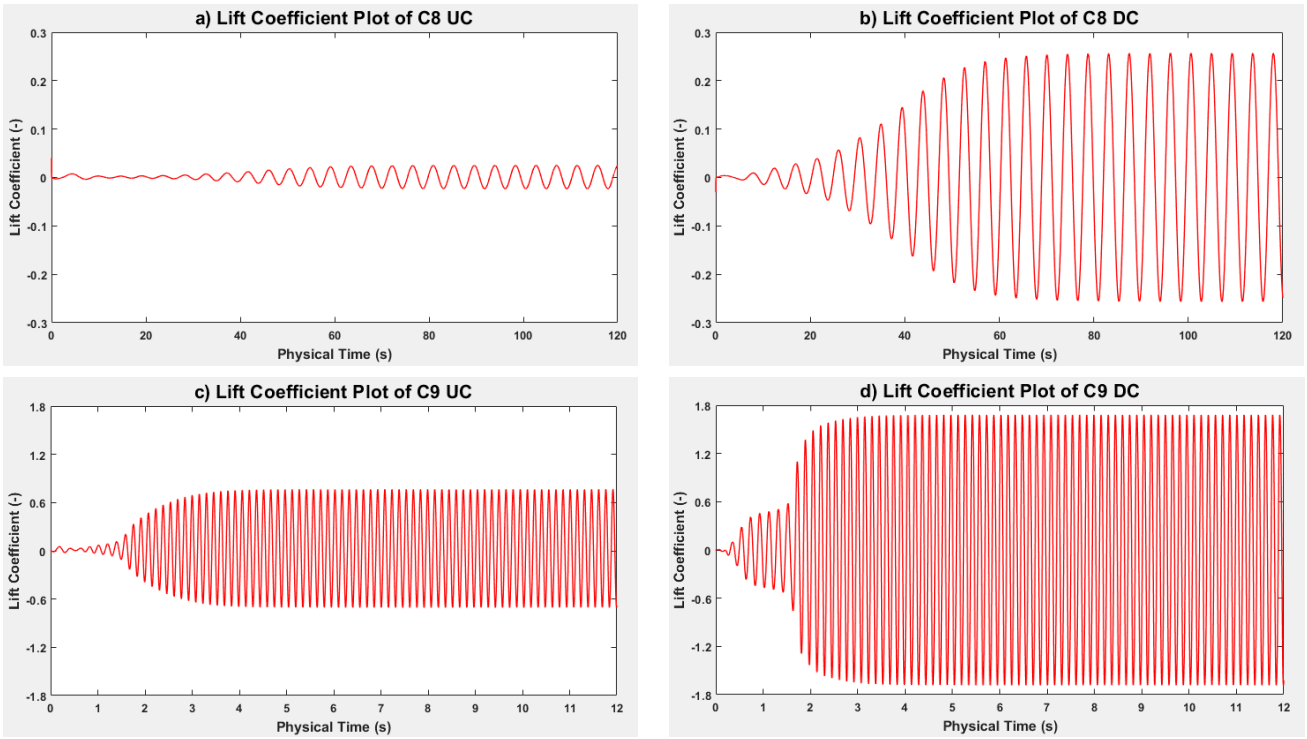

Figure S10. *Lift coefficient plot of a) C8 UC at Re = 200; b) C8 DC at Re = 200; c) C9 UC at Re = 3900; d) C9 DC at Re = 3900.*

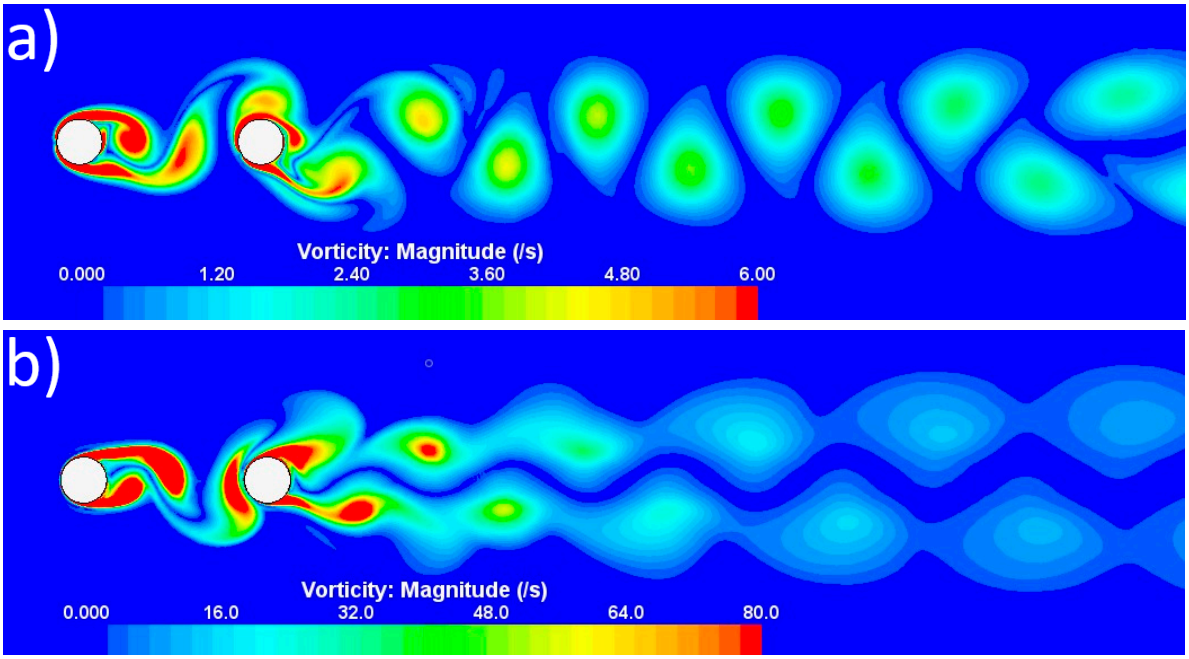

Figure S11. *Vorticity contours of a) C10 at Re = 200; b) C11 at Re = 3900.*

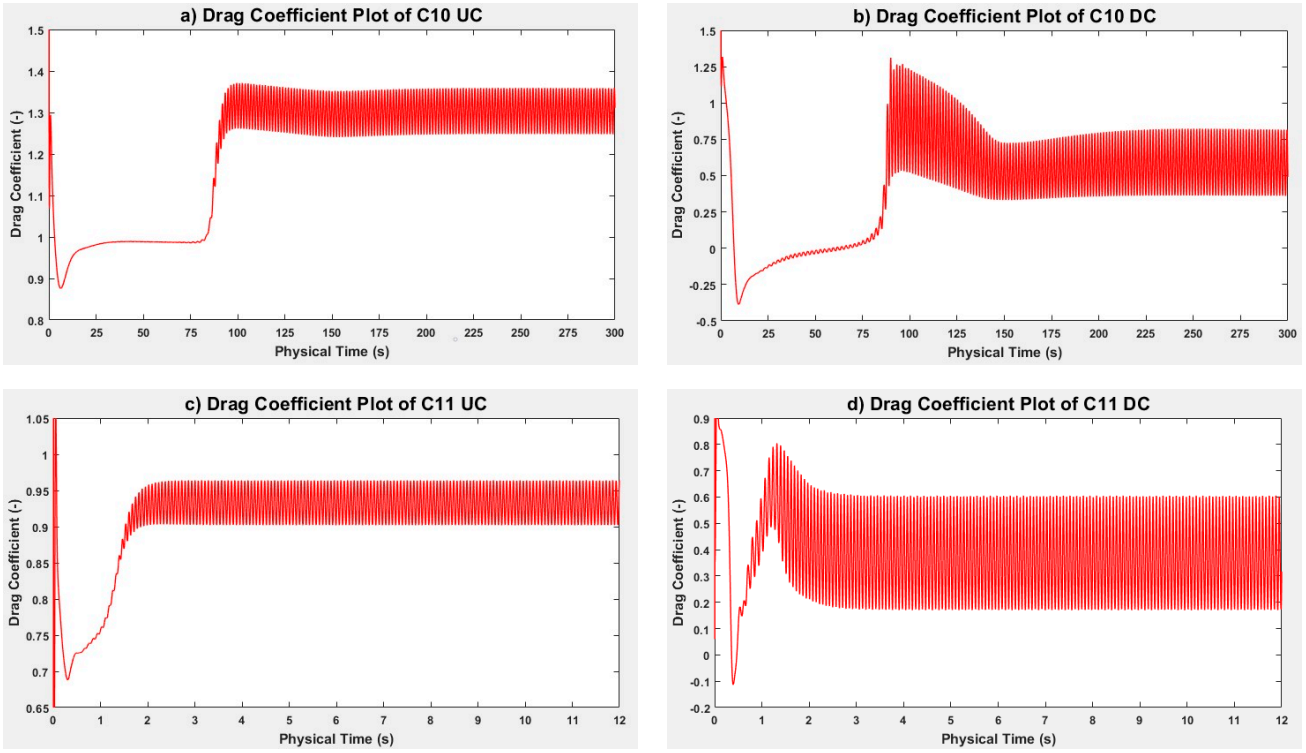

Figure S12. *Drag coefficient plot of a) C10 UC at Re = 200; b) C10 DC at Re = 200; c) C11 UC at Re = 3900; d) C11 DC at Re = 3900.*

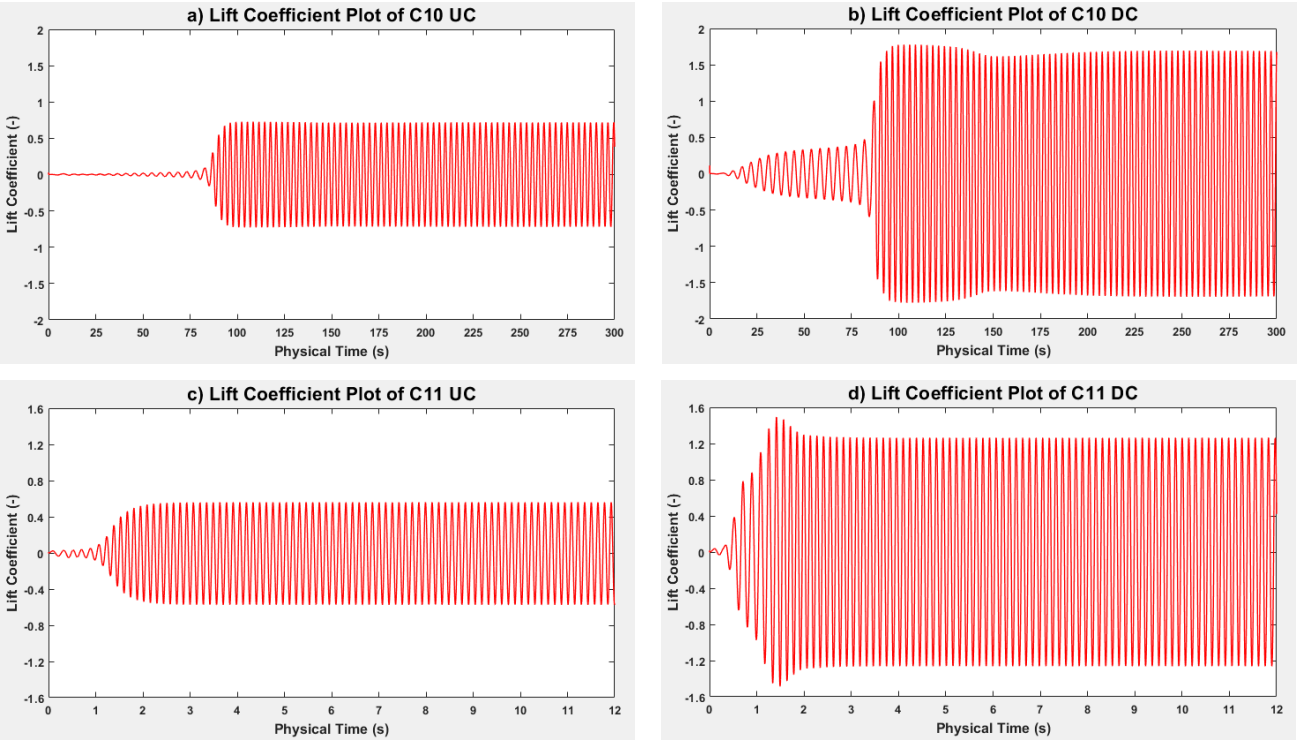

Figure S13. *Lift coefficient plot of a) C10 UC at Re = 200; b) C10 DC at Re = 200; c) C11 UC at Re = 3900; d) C11 DC at Re = 3900.*

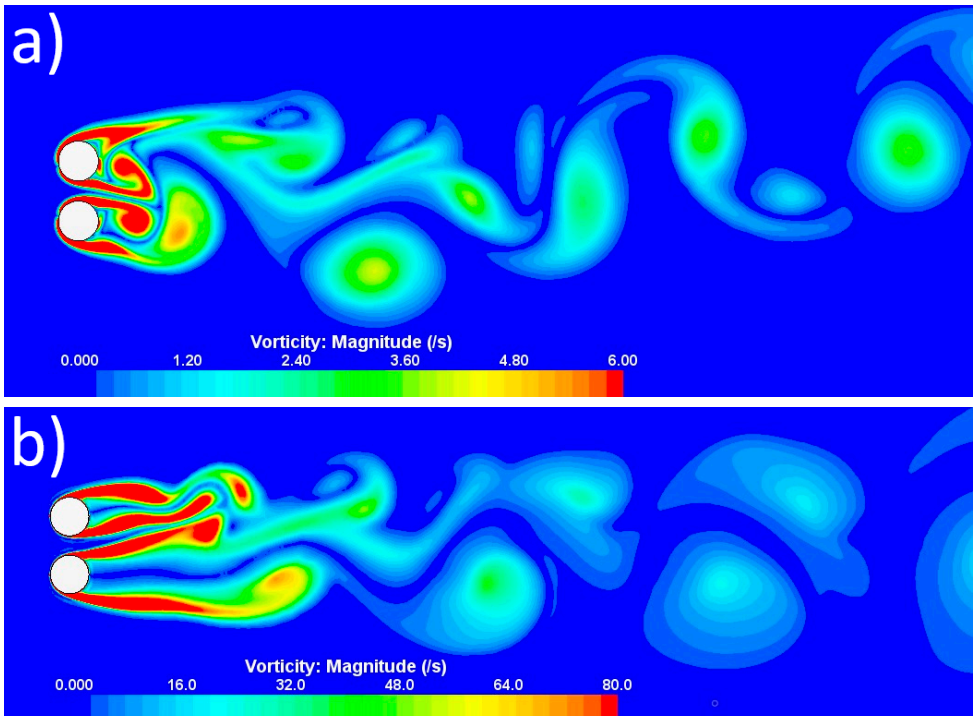

Figure S14. *Vorticity contours of a) C12 at Re = 200; b) C13 at Re = 3900.*

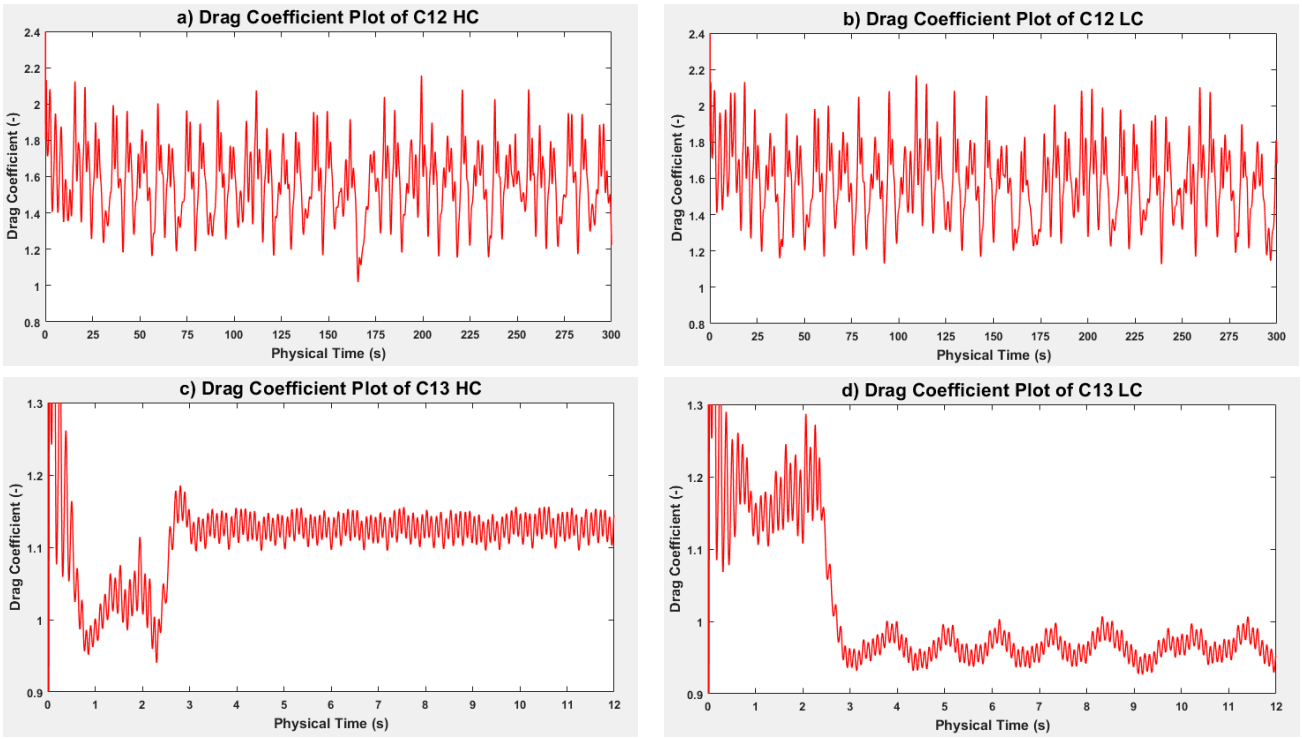

Figure S15. *Drag coefficient plot of a) C12 HC at Re = 200; b) C12 LC at Re = 200; c) C13 HC at Re = 3900; d) C13 LC at Re = 3900.*

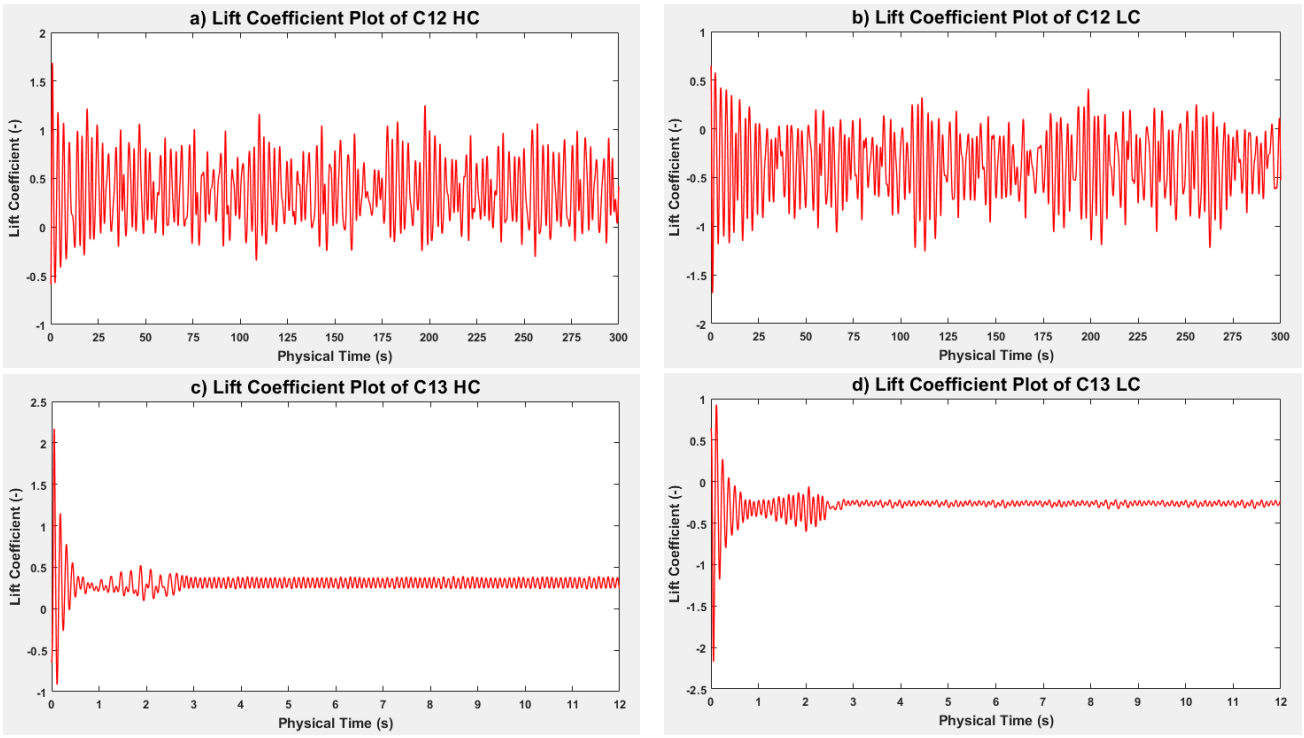

Figure S16. *Lift coefficient plot of a) C12 HC at Re = 200; b) C12 LC at Re = 200; c) C13 HC at Re = 3900; d) C13 LC at Re = 3900.*

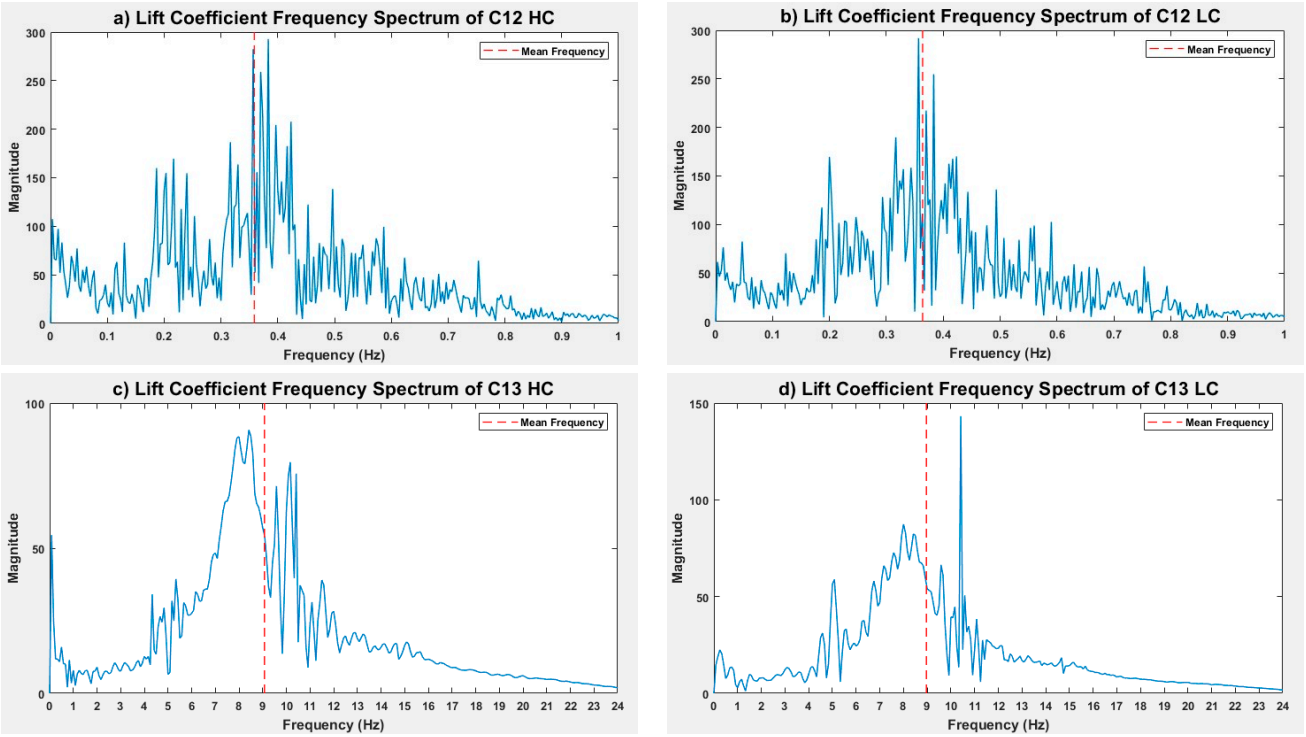

Figure S17. *Lift coefficient frequency spectrum plot of a) C12 HC at* $Re = 200$*; b) C12 LC at* $Re = 200$*; c) C13 HC at* $Re = 3900$*; d) C13 LC at* $Re = 3900$*.*

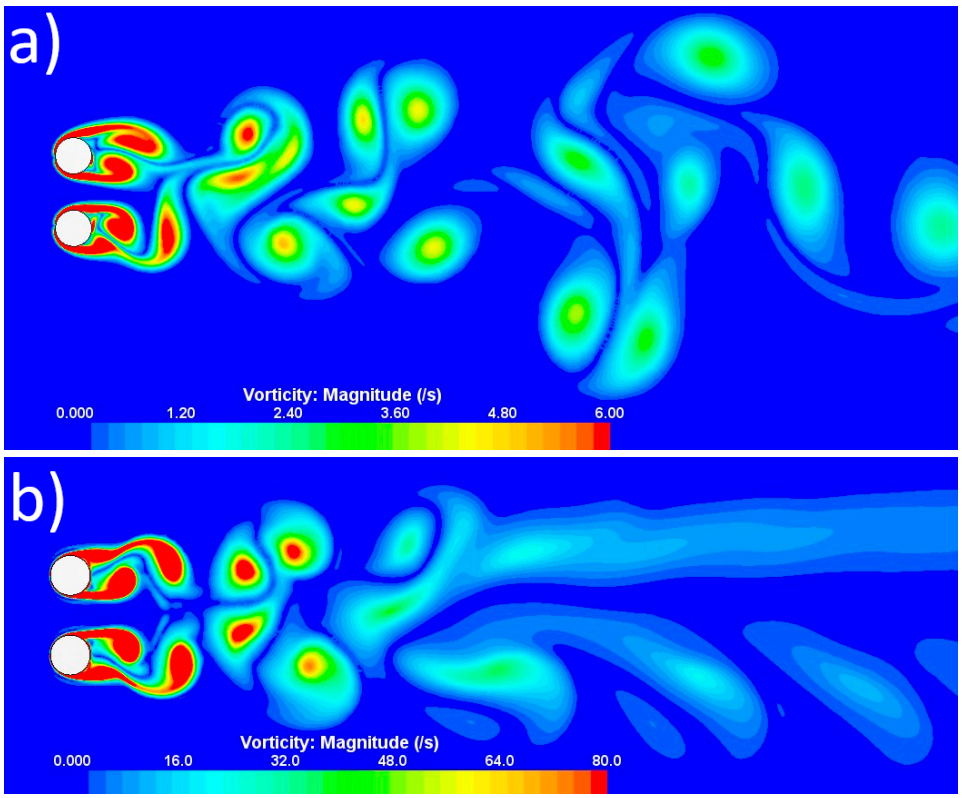

Figure S18. *Vorticity contours of a) C14 at* $Re = 200$*; b) C15 at* $Re = 3900$*.*

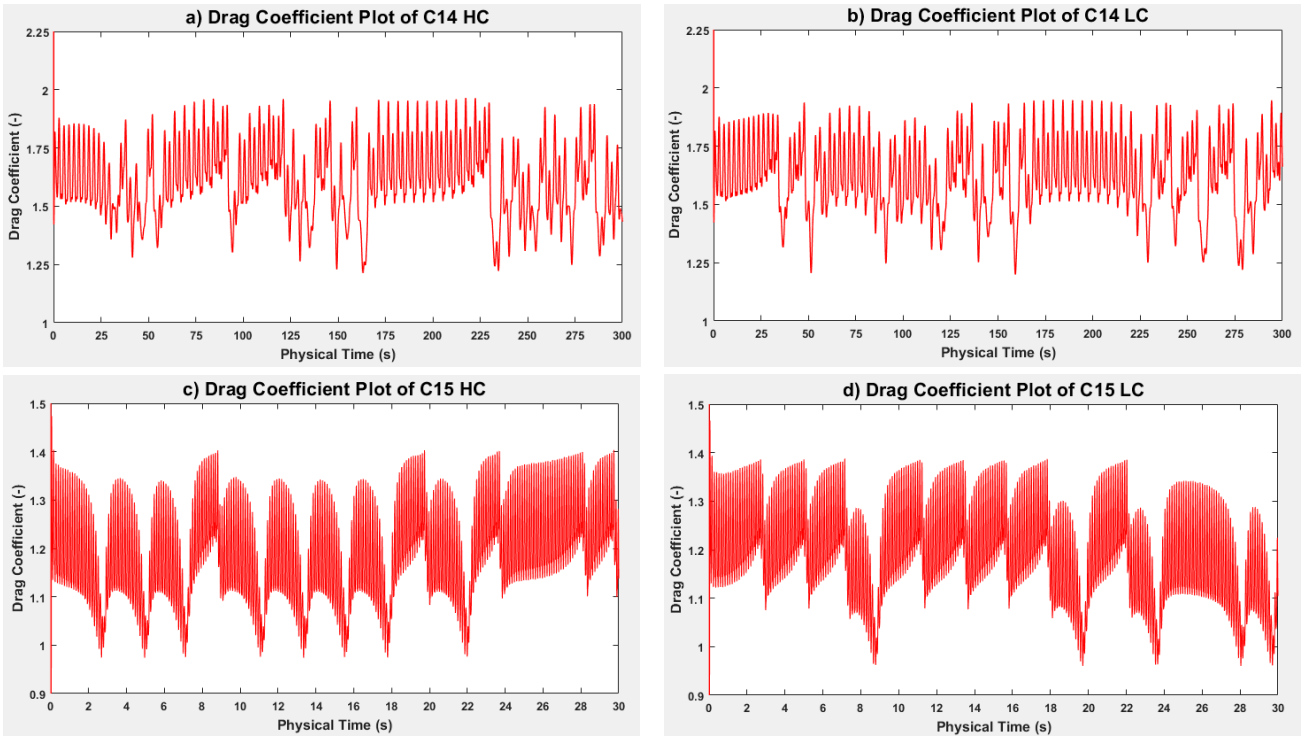

Figure S19. *Drag coefficient plot of a) C14 HC at* $Re = 200$*; b) C14 LC at* $Re = 200$*; c) C15 HC at* $Re = 3900$*; d) C15 LC at* $Re = 3900$*.*

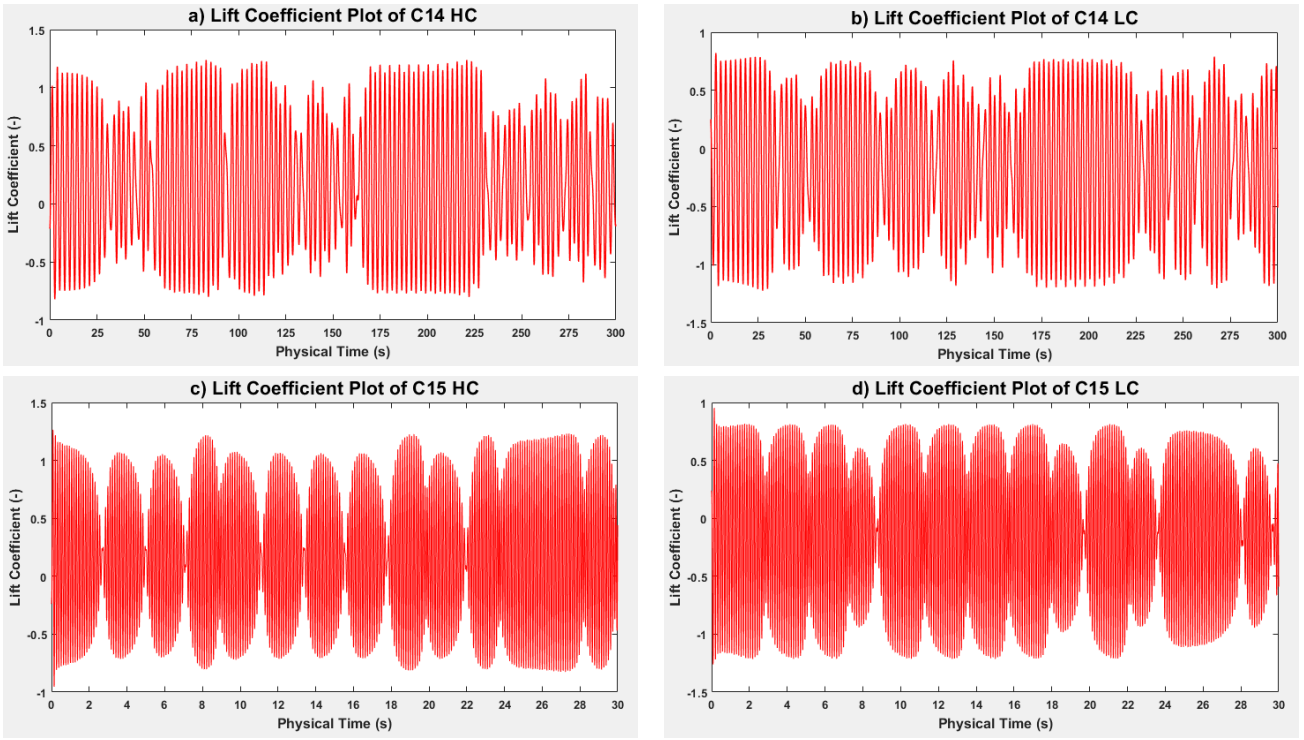

Figure S20. *Lift coefficient plot of a) C14 HC at* $Re = 200$*; b) C14 LC at* $Re = 200$*; c) C15 HC at* $Re = 3900$*; d) C15 LC at* $Re = 3900$*.*

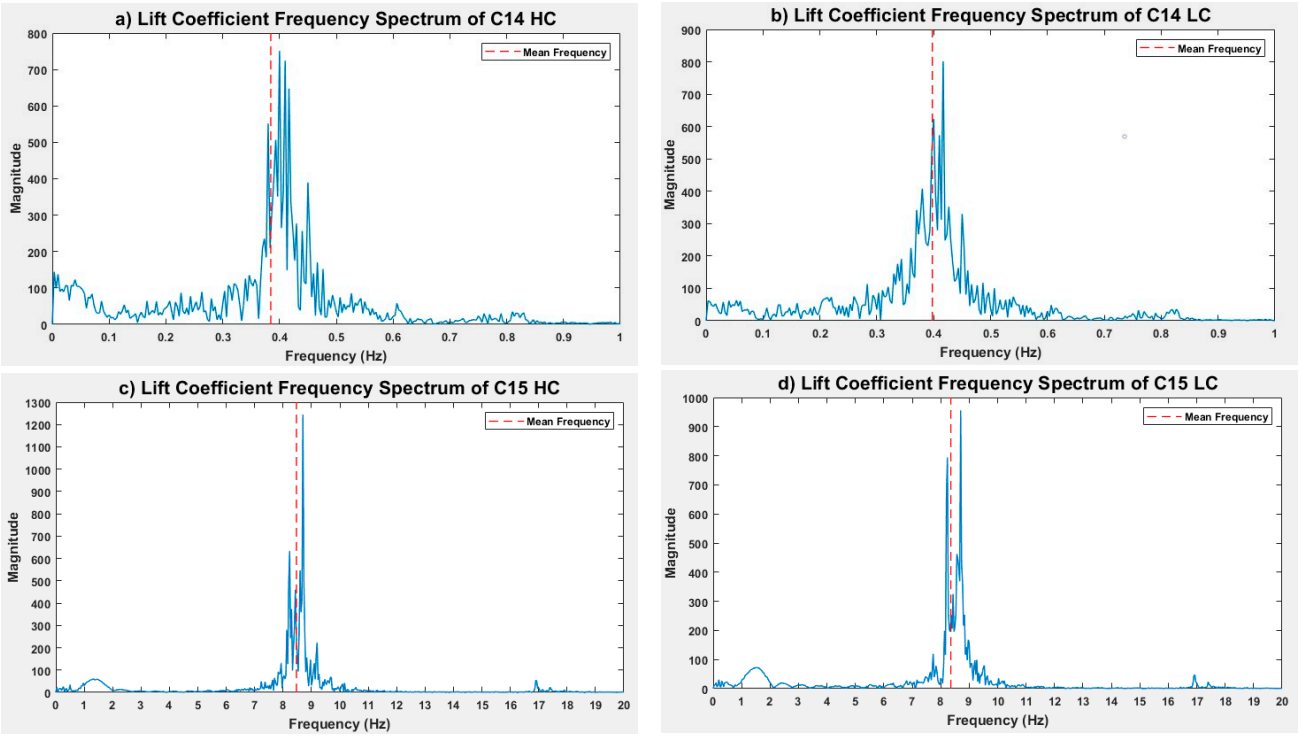

Figure S21. *Lift coefficient frequency spectrum plot of a) C14 HC at* $Re = 200$*; b) C14 LC at* $Re = 200$*; c) C15 HC at* $Re = 3900$*; d) C15 LC at* $Re = 3900$*.*

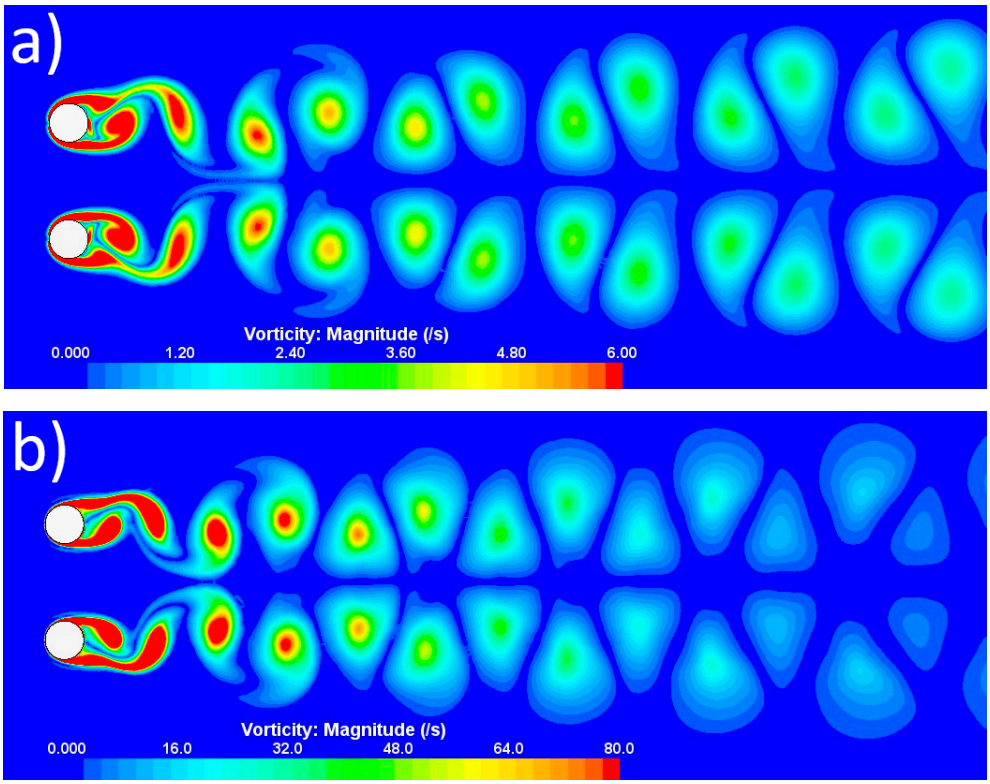

Figure S22. *Vorticity contours of a) C16 at* $Re = 200$*; b) C17 at* $Re = 3900$*.*

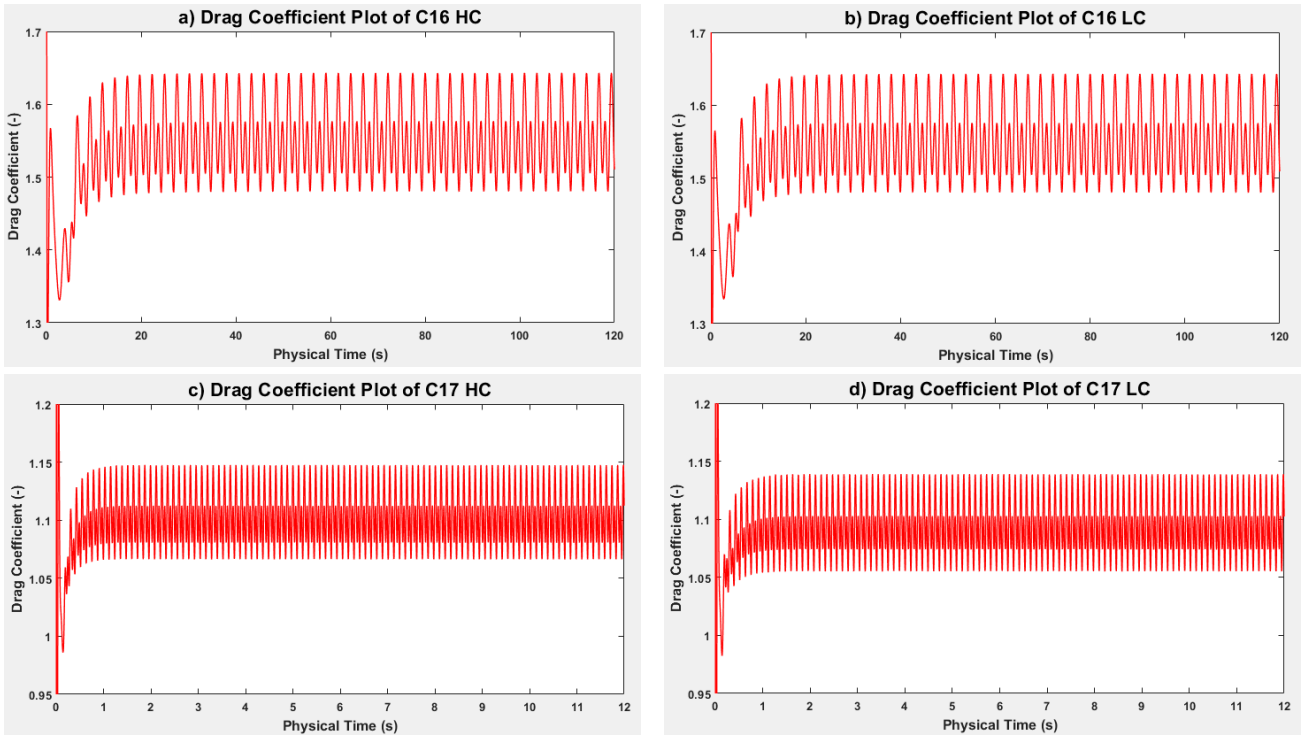

Figure S23. *Drag coefficient plot of a) C16 HC at Re = 200; b) C16 LC at Re = 200; c) C17 HC at Re = 3900; d) C17 LC at Re = 3900.*

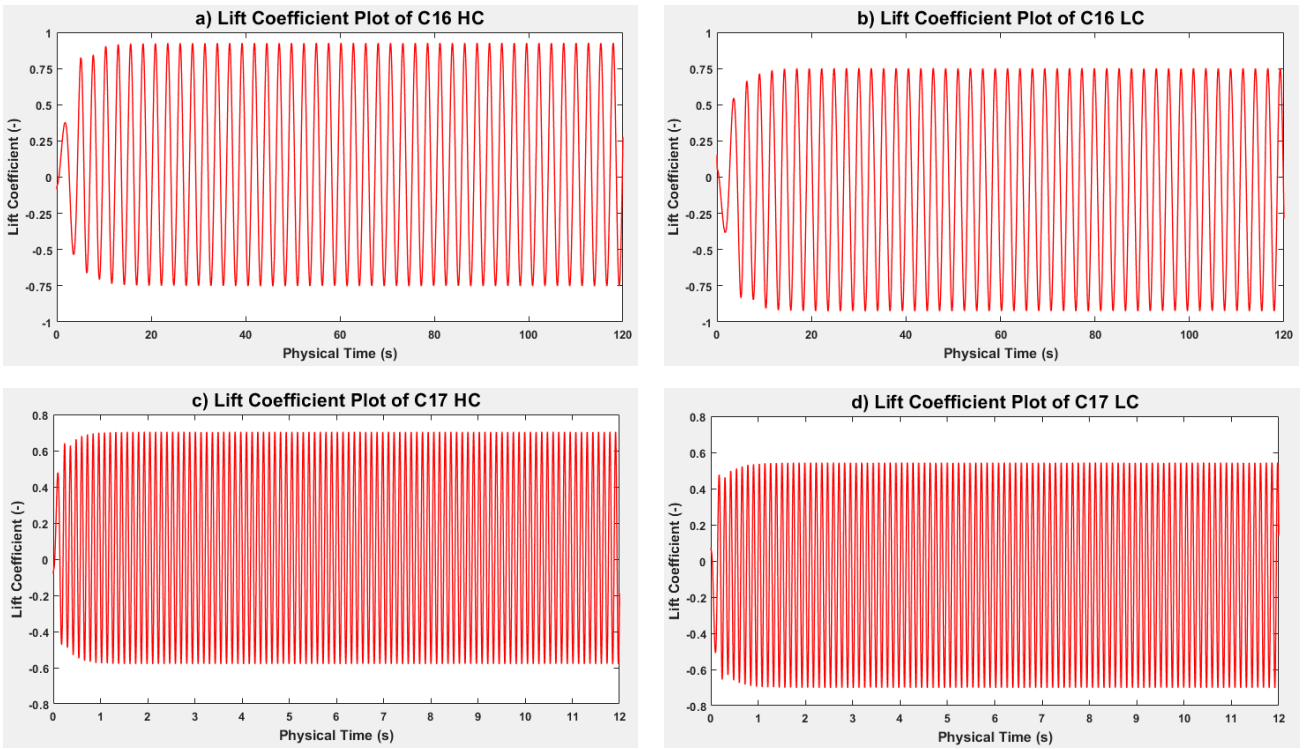

Figure S24. *Lift coefficient plot of a) C16 HC at Re = 200; b) C16 LC at Re = 200; c) C17 HC at Re = 3900; d) C17 LC at Re = 3900.*

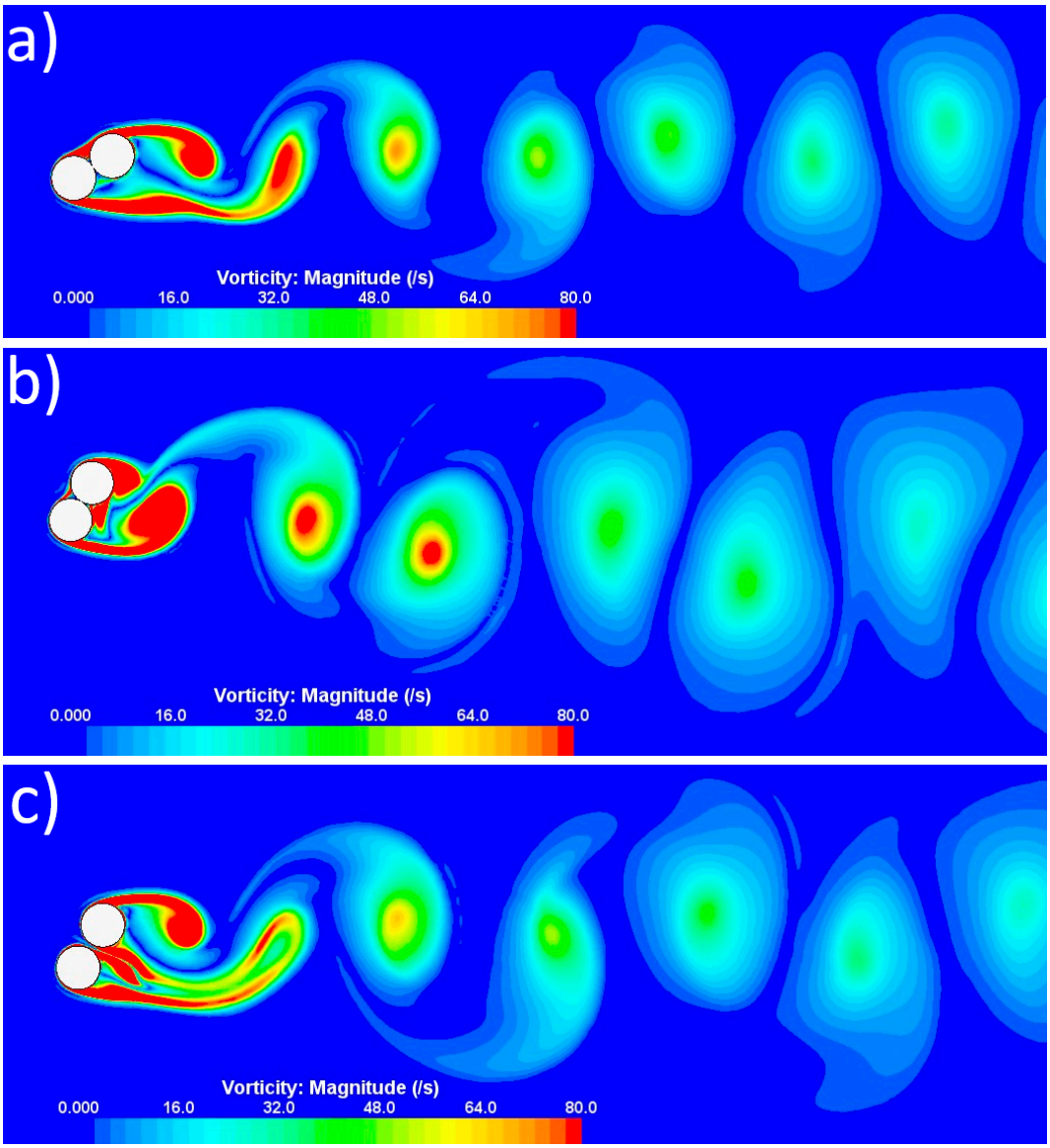

Figure S25. *Vorticity contours of single bluff-body flow patterns at* $Re = 3900$ *of a) C18 at* $\frac{P}{D} = 1.0, \alpha = 30°$*; b) C19 at* $\frac{P}{D} = 1.0, \alpha = 60°$ *; c) C20 at* $\frac{P}{D} = 1.125, \alpha = 60°$.

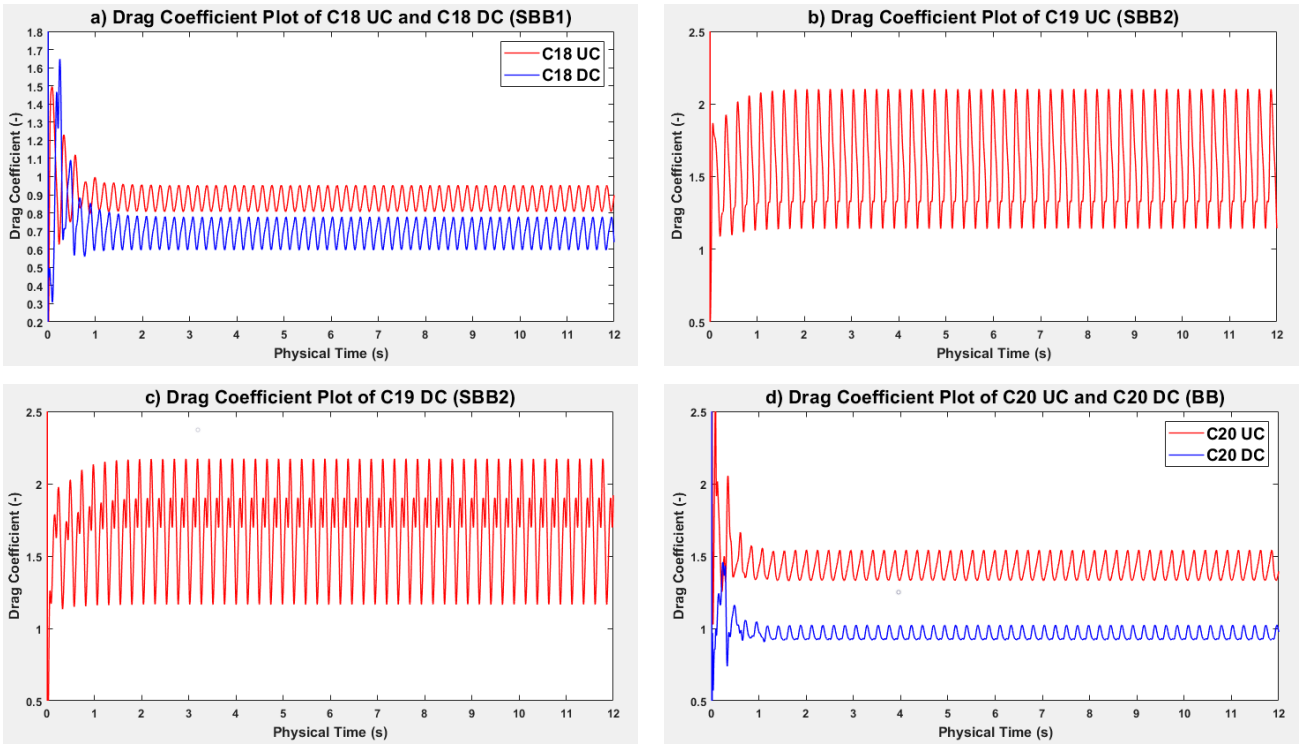

Figure S26. *Drag coefficient plot at* $Re = 3900$ *of a) C18; b) C19 UC; c) C19 DC; d) C20.*

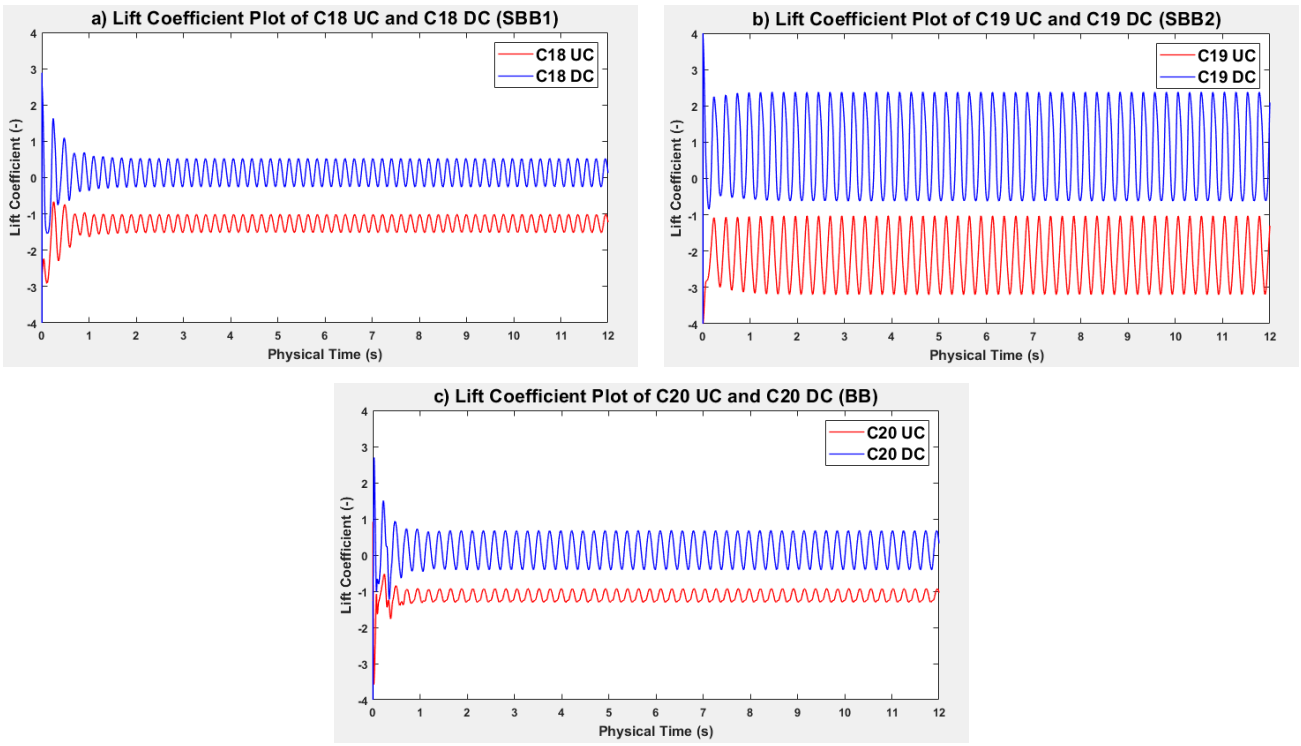

Figure S27. *Lift coefficient plot at* $Re = 3900$ *of a) C18; b) C19; c) C20.*

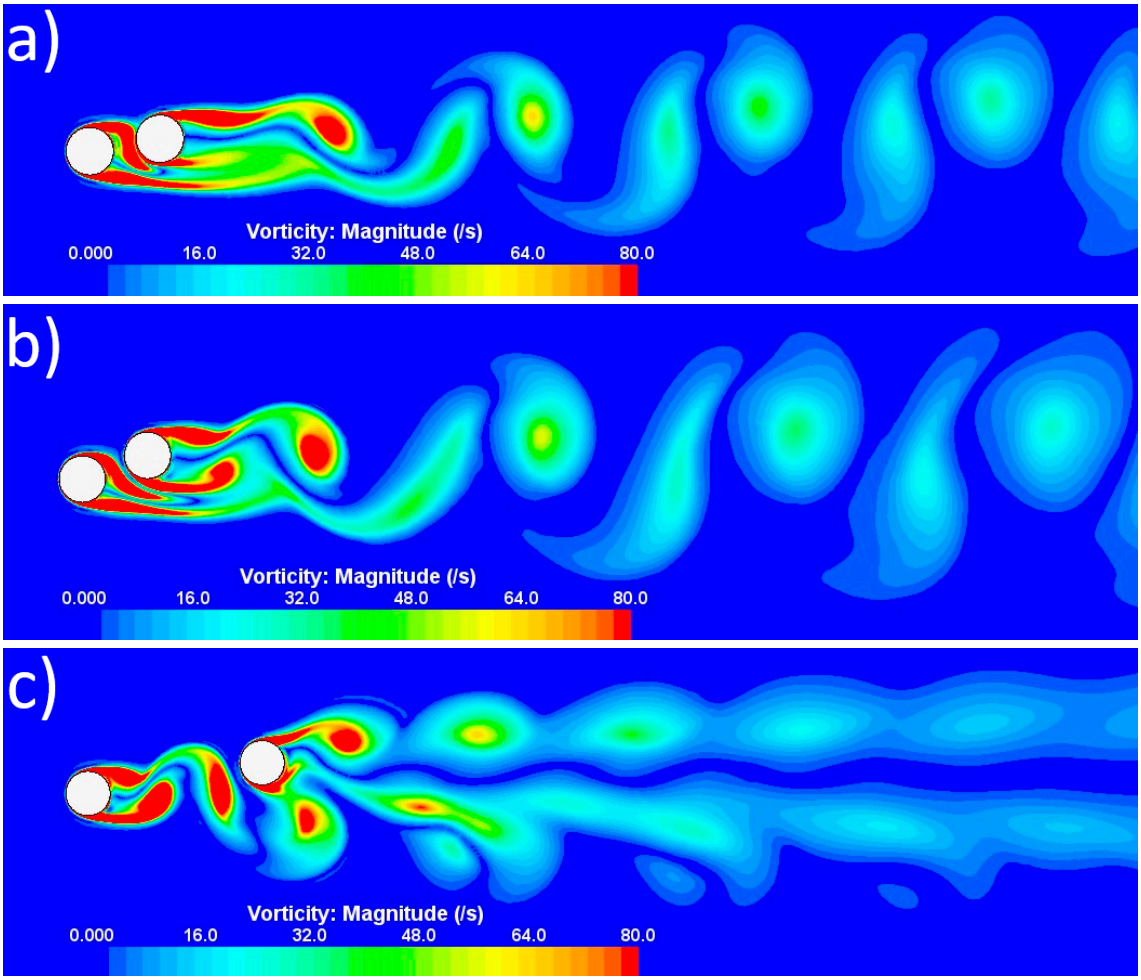

Figure S28. *Vorticity contours of small-incidence-angle flow patterns at* $Re = 3900$ *of a) C21 at* $\frac{P}{D} = 1.5, \alpha = 10°$*; b) C22 at* $\frac{P}{D} = 1.5, \alpha = 20°$ *; c) C23 at* $\frac{P}{D} = 4.0, \alpha = 10°$.

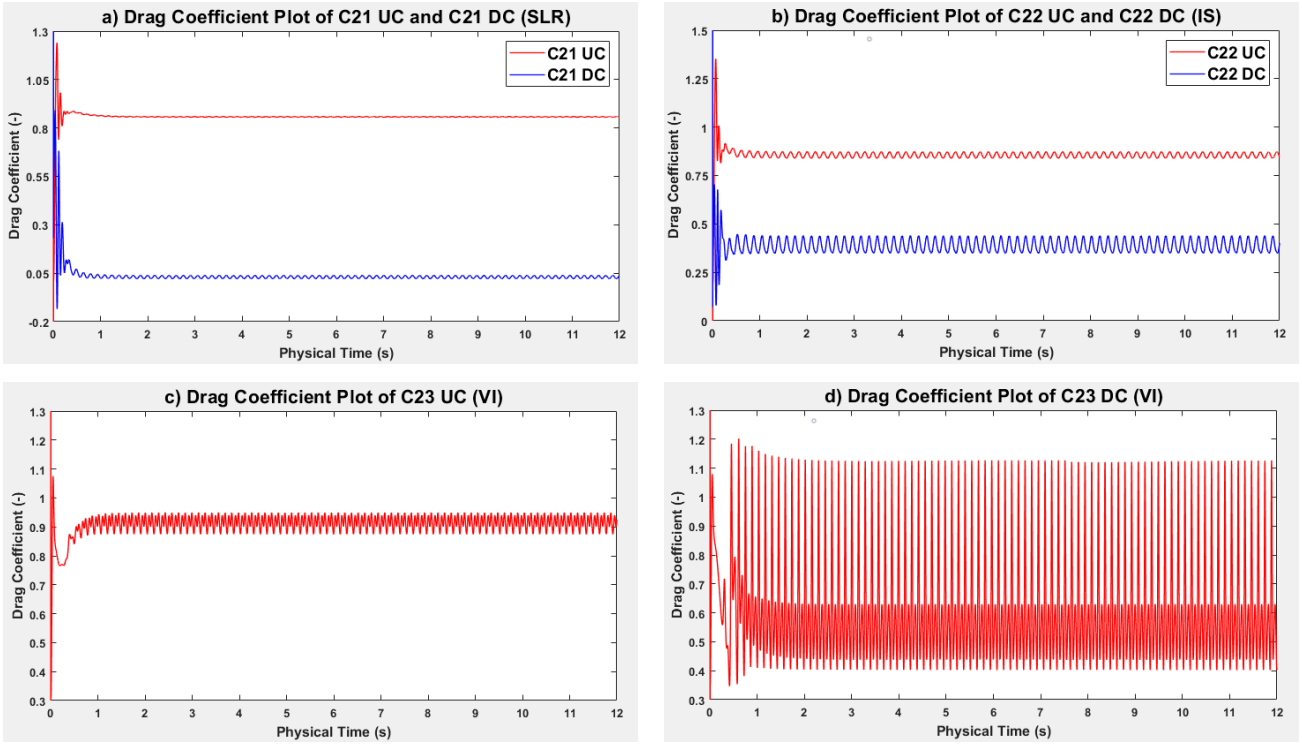

Figure S29. *Drag coefficient plot at* $Re = 3900$ *of a) C21; b) C22; c) C23 UC; d) C23 DC.*

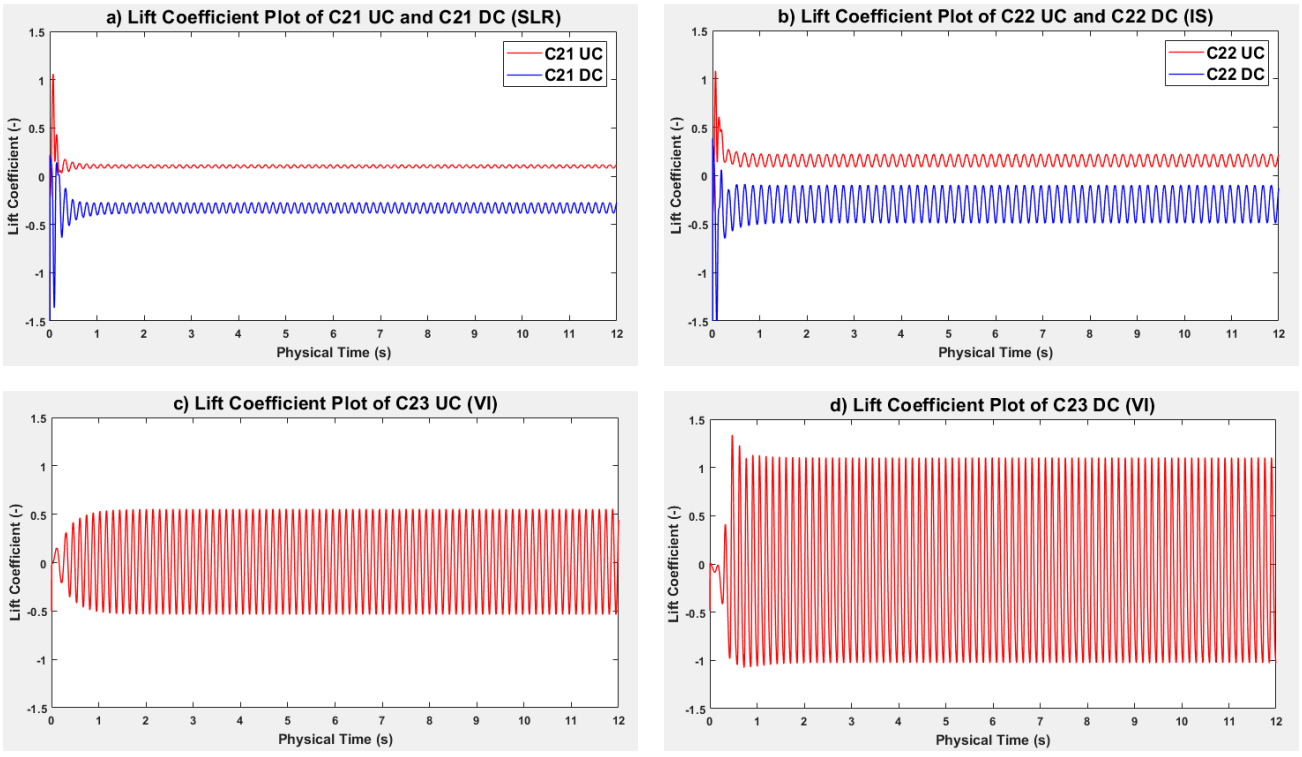

Figure S30. *Lift coefficient plot at* $Re = 3900$ *of a) C21; b) C22; c) C23 UC; d) C23 DC.*

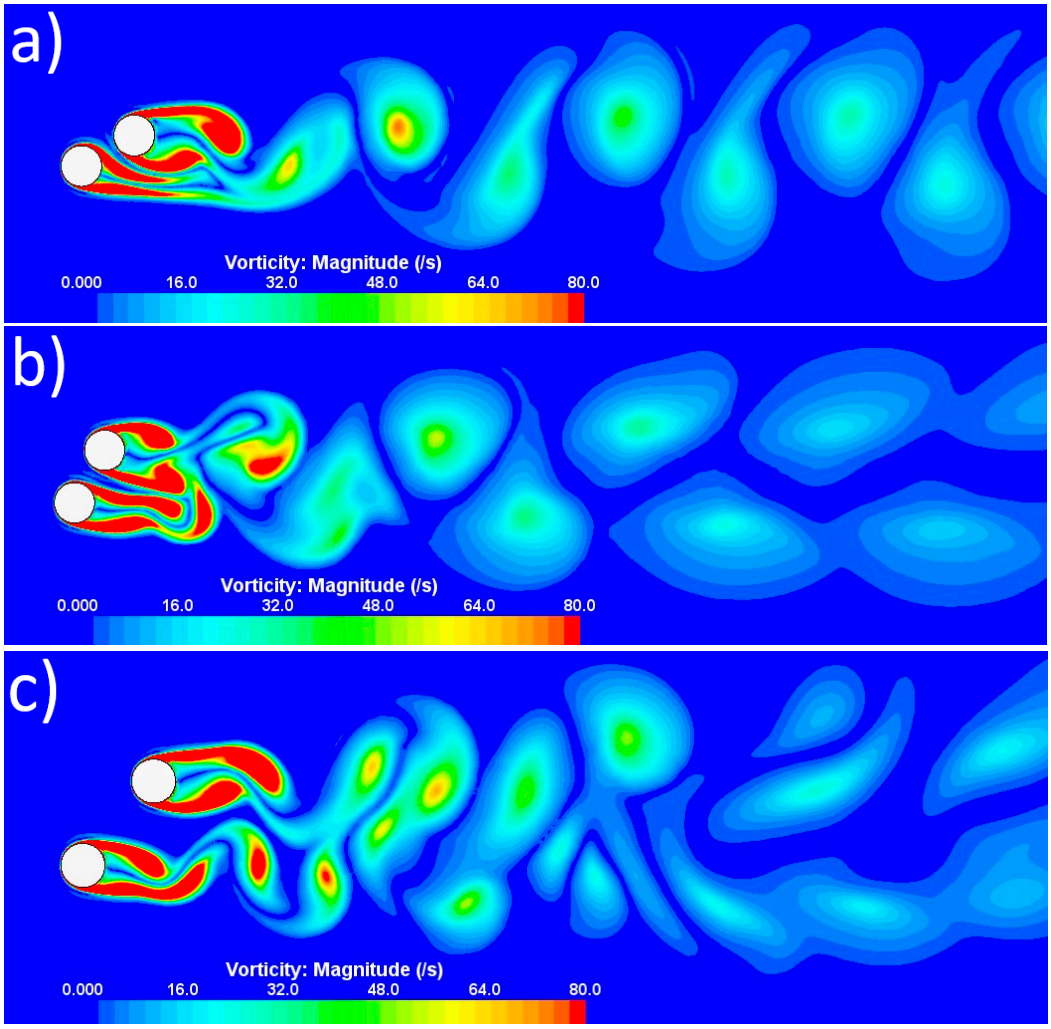

Figure S31. *Vorticity contours of large-incidence-angle flow patterns at* $Re = 3900$ *of a) C24 at* $\frac{P}{D} = 1.5, \alpha = 30°$*; b) C25 at* $\frac{P}{D} = 1.5, \alpha = 60°$ *; c) C26 at* $\frac{P}{D} = 2.5, \alpha = 50°$.

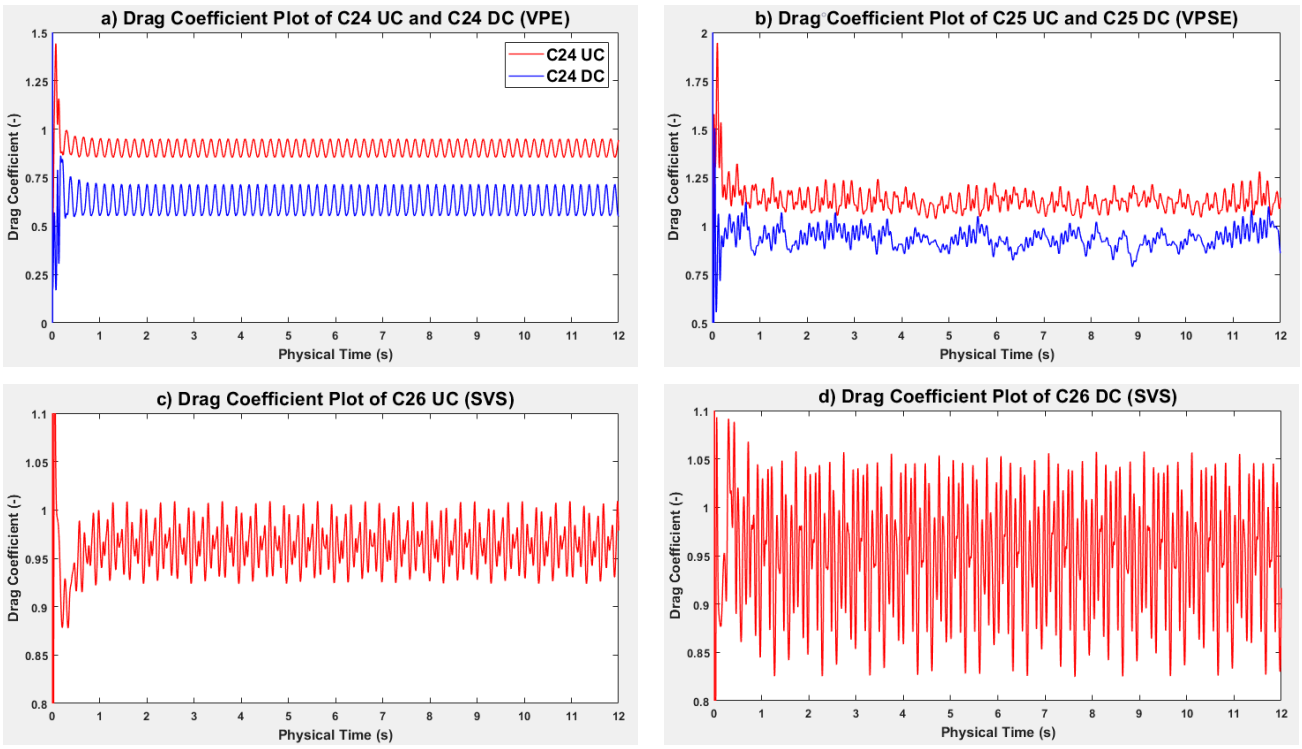

Figure S32. *Drag coefficient plot at* $Re = 3900$ *of a) C24; b) C25; c) C26 UC; d) C26 DC.*

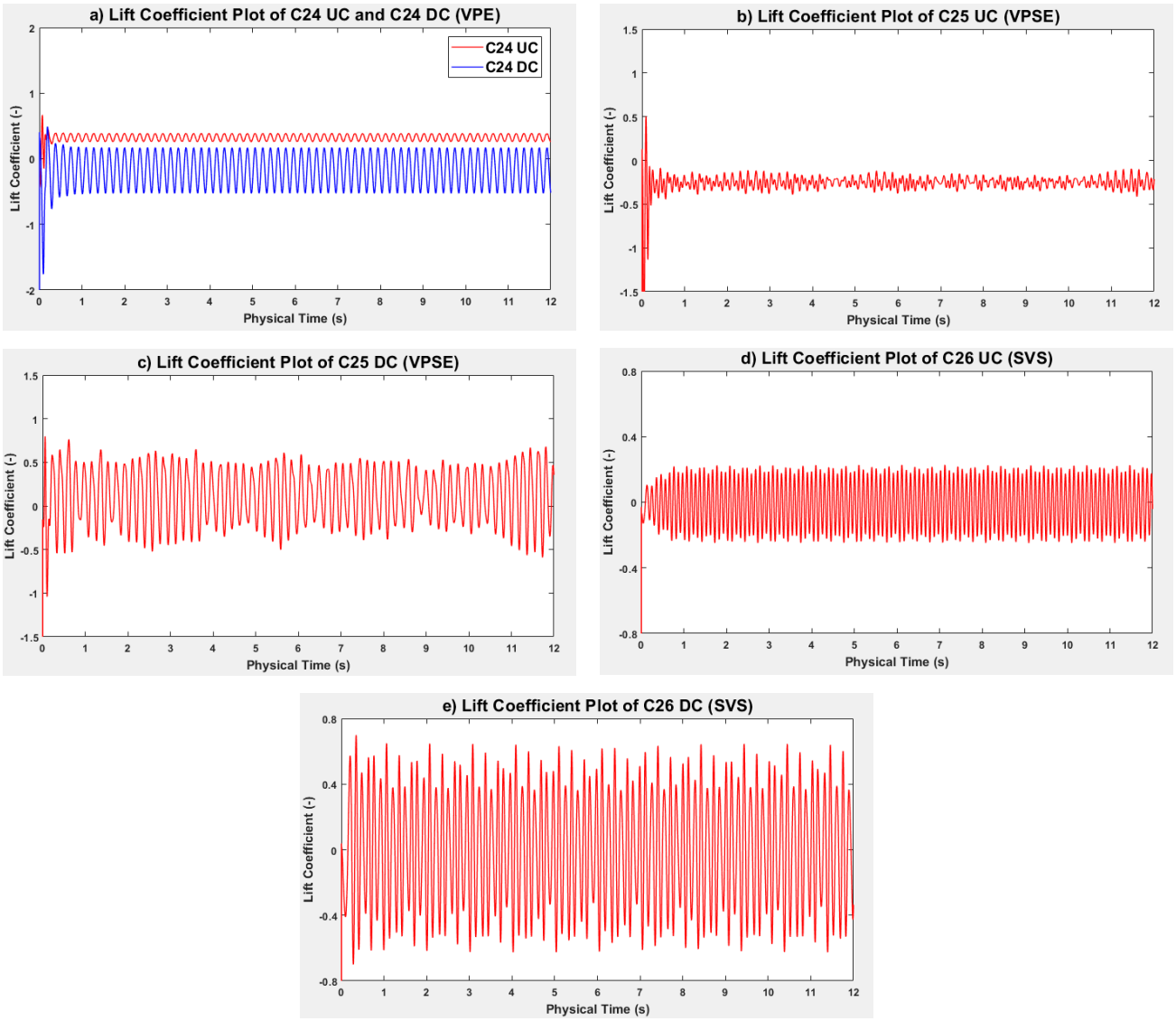

Figure S33. *Lift coefficient plot at* $Re = 3900$ *of a) C24; b) C25 UC; c) C25 DC; d) C26 UC; e) C26 DC.*

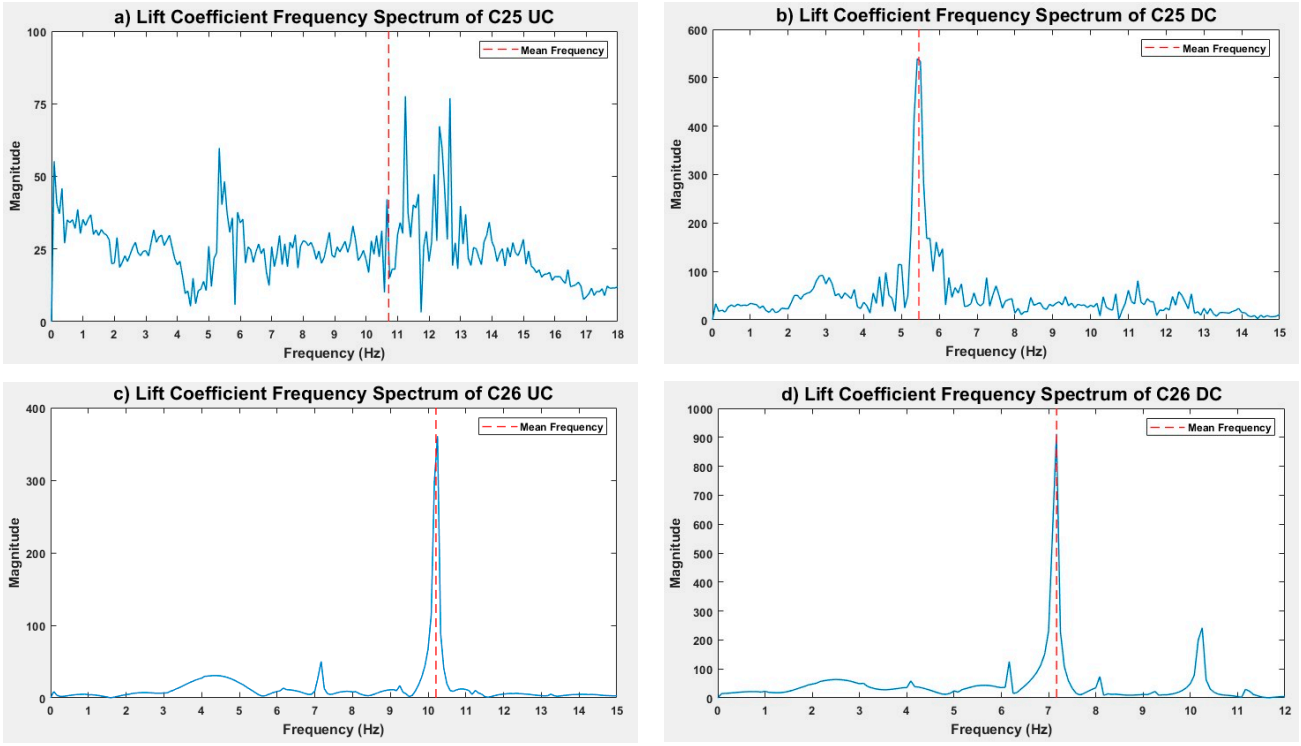

Figure S34. *Lift coefficient frequency spectrum plot at* $Re = 3900$ *of a) C25 UC; b) C25 DC; c) C26 UC; d) C26 DC.*

Additional tandem simulations at $Re = 3900$, AS1 and AS2 for $\frac{L}{D} = 1.25$ and $\frac{L}{D} = 1.025$ are shown in Figure S35 (a) and Figure S35 (b), respectively. In AS1, there are visible vortices between the cylinders, and the shear layers from UC reattach onto the DC. In AS2, the gap is significantly reduced but the fluid between the cylinders is not stagnant. The wake resembles a single-cylinder case and the distance between vortices is decreased, which indicates increased f_s. However, the shear layers from UC still reattach onto the DC.

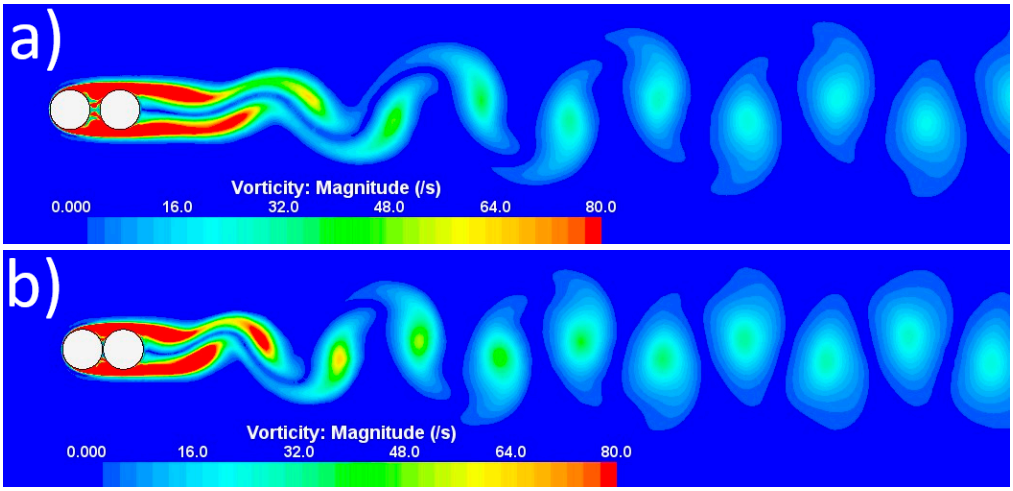

Figure S35. *Vorticity contours at* $Re = 3900$ *of a) AS1; b) AS2.*

The C_d of all cylinders in the additional study have negligible fluctuations. The C_l fluctuations are stable, with higher amplitude in AS2, for both cylinders. In AS1, $\overline{C_{d_{DC}}}$ and $\overline{C_{d_{UC}}}$ are insignificantly lower than in AS2. The C_d plots of AS1 and AS2 are shown in Figure S36 (a) and Figure S36 (b), respectively. The C_l plots of AS1 and AS2 are shown in Figure S37. The numerical values are shown in Table S1.

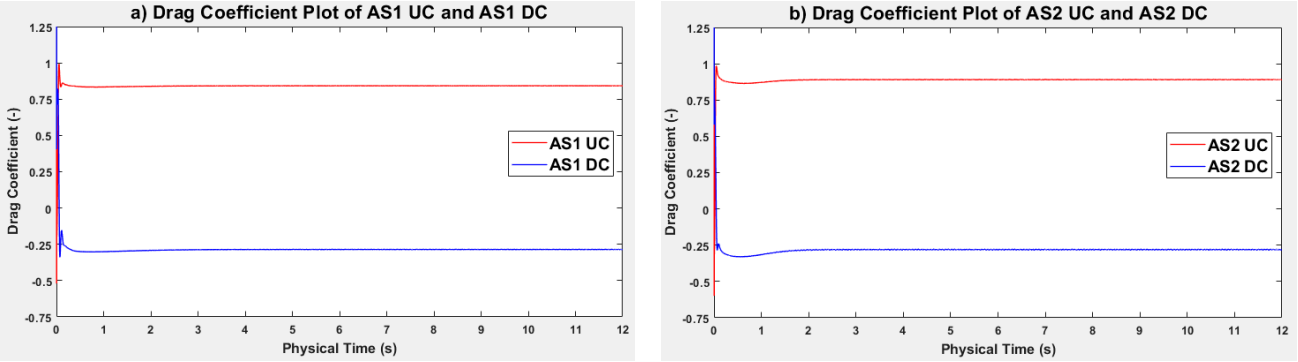

Figure S36. *Drag coefficient plot at* $Re = 3900$ *of a) AS1; b) AS2.*

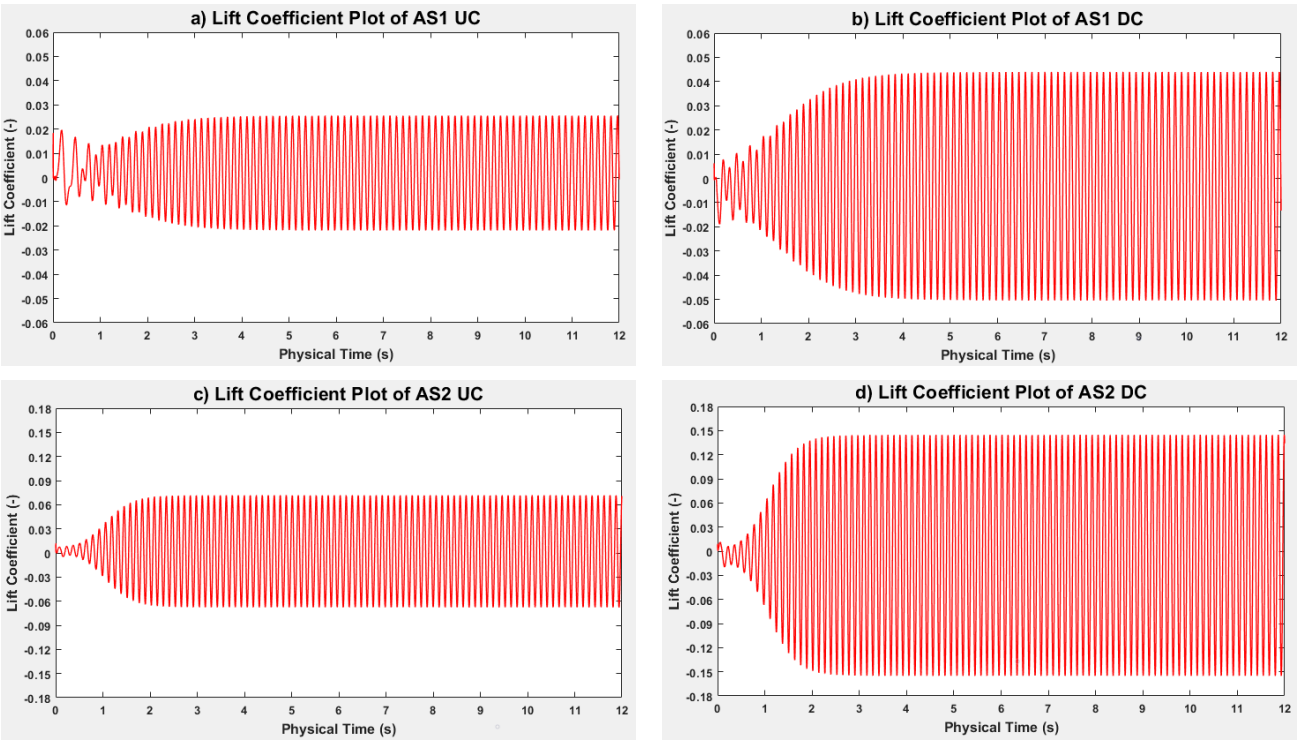

Figure S37. *Lift coefficient plot at* $Re = 3900$ *of a) AS1 UC; b) AS1 DC; c) AS2 UC; d) AS2 DC.*

Table S1. *Numerical results of C_d and St for AS1 and AS2 at $Re = 3900$, in the flow around two cylinders, in tandem arrangement.*

Gap L	1.25 D (AS1)				1.025 D (AS2)			
Parameter	$\overline{C_{d_{DC}}}$	$\overline{C_{d_{UC}}}$	St_{UC}	St_{DC}	$\overline{C_{d_{DC}}}$	$\overline{C_{d_{DC}}}$	St_{UC}	St_{DC}
Values	0.84	-0.285	0.209	0.209	0.89	-0.28	0.227	0.227